Elsevier Editorial System(tm) for Free Radical Biology and Medicine

Manuscript Draft

Manuscript Number: FRBM-D-16-00676R1

Title: The antioxidant uncoupling protein 2 stimulates hnRNPA2/B1, GLUT1 and PKM2 expression and sensitizes pancreas cancer cells to glycolysis inhibition

Article Type: Original article

Keywords: cancer; metabolism; uncoupling proteins; UCP2; Warburg effect; proteomics.

Corresponding Author: Dr. Massimo Donadelli, Ph.D.

Corresponding Author's Institution: University of Verona

First Author: Jessica Brandi

Order of Authors: Jessica Brandi; Daniela Cecconi; Marco Cordani; Margalida Torrens-Mas; Raffaella Pacchiana; Elisa Dalla Pozza; Giovanna Butera; Marcello Manfredi; Emilio Marengo; Jordi Oliver; Pilar Roca; Ilaria Dando, PhD; Massimo Donadelli, Ph.D.

Abstract: Several evidence indicate that metabolic alterations play a pivotal role in cancer development. Here, we report that the mitochondrial uncoupling protein 2 (UCP2) sustains the metabolic shift from mitochondrial oxidative phosphorylation (mtOXPHOS) to glycolysis in pancreas cancer cells. Indeed, we show that UCP2 sensitizes pancreas cancer cells to the treatment with the glycolytic inhibitor 2-deoxy-D-glucose. Through a bidimensional electrophoresis analysis, we identify 19 protein species differentially expressed after treatment with the UCP2 inhibitor genipin and, by bioinformatic analyses, we show that these proteins are mainly involved in metabolic processes. In particular, we demonstrate that the antioxidant UCP2 induces the expression of hnRNPA2/B1, which is involved in the regulation of both GLUT1 and PKM2 mRNAs, and of lactate dehydrogenase (LDH) increasing the secretion of L-lactic acid. We further demonstrate that the radical scavenger N-acetyl-L-cysteine reverts hnRNPA2/B1 and PKM2 inhibition by genipin indicating a role for reactive oxygen species in the metabolic reprogramming of cancer cells mediated by UCP2. We also observe an UCP2-dependent decrease in mtOXPHOS complex I (NADH dehydrogenase), complex IV (cytochrome c oxidase), complex V (ATPase) and in mitochondrial oxygen consumption, suggesting a role for UCP2 in the counteraction of pancreatic cancer cellular respiration. All these results reveal novel mechanisms through which UCP2 promotes cancer cell proliferation with the concomitant metabolic shift from mtOXPHOS to the glycolytic pathway.

UNIVERSITÀ di VERONA
Dipartimento di NEUROSCIENZE, BIOMEDICINA E MOVIMENTO

**Free Radical Biology & Medicine** Verona, October 12th 2016

Editorial Office

Dear Prof. Enrique Cadenas,

we wish to thank you very much for your efforts in handling our manuscript (FRBM-D-16-00676) and for giving us the opportunity to revise and improve it. We greatly appreciated your thoughtful and those from the reviewers. We revised the manuscript accordingly.

*Dear Dr. Donadelli,*

*Thank you for submitting the above-mentioned article to Free Radical Biology & Medicine.*

*We have completed the review of your manuscript and a summary is enclosed below. Although the manuscript cannot be accepted for publication in its present form, appropriate responses to the suggested revisions would make it reasonable to reconsider. At this point, I would ask you to consider revising your manuscript as per the comments. The manuscript would then be returned to the reviewers for their reconsideration. Please understand that there is no guarantee that simple revision or rebuttal will be sufficient as additional experiments or other major changes may be required.*

As required by Reviewers, we have revised the manuscript re-organizing the data reported and presenting the results in a chronological order starting from the simplest data. Thus, we have modified the manuscript in order to help the reader to keep the overall aim of the study. Accordingly with the modifications of the text we have also re-organized the order of the figures. As required by Reviewers we have also performed additional experiments. The new results have been inserted in the main figures and properly discussed in the text.

Yours sincerely,

Massimo Donadelli

Ilaria Dando

**Dipartimento di Neuroscienze, Biomedicina e Movimento**
Piazzale Ludovico Antonio Scuro, 10 – 37134 VERONA – Policlinico "G.B. Rossi" | T +39 045 8124287
P. IVA 01541040232 | C.F. 93009870234

UNIVERSITÀ di VERONA
Dipartimento di NEUROSCIENZE, BIOMEDICINA E MOVIMENTO

**Free Radical Biology & Medicine** Verona, October 12th 2016

Editorial Office

Dear Prof. Enrique Cadenas,

below please find the detailed, itemized list of our responses to the Reviewers' suggestions/comments and the changes we have made in the revised version of the manuscript.

**Reviewers' comments:**

*Reviewer #2: The manuscript by Brandi et al has investigated the metabolic role of antioxidant uncoupling protein 2 in pancreas cancer cells. The authors demonstrate that down regulation of UCP2 by pharmacological inhibitor or si RNA induced alterations in the mitochondrial function, redox dynamics and glycolytic parameters in cancer cells. The authors have carried out 2D gel based proteomic analysis followed by identification and validation of differentially expressed proteins including hnRNPA2/B1, which regulates the expression of down-stream genes including GLUT1 and PKM2. Based on the proteomics data, the authors have attempted to explain the pathophysiological effects of UCP2 down-regulation and over expression in cancer cells. The authors also use the model to explain the importance of glycolytic regulation and mitochondrial dynamics in cancer progression.*

*Following are the comments regarding the study:*

*1. Although the objective of the study is good and relevant experiments have been conducted generating important results, the organization of the data is haphazard and makes it difficult for the readers. I request the authors to present the results in a chronological order starting from the simplest data. The authors start out by mentioning figures 3B, 4A and 5A. Also, instead of presenting the preliminary data in the supplementary section, please present in the main figures. In fact, fig 1 in the current version could go into supplementary section.*

*First show knock-down or inhibition of UCP2 followed by analysis of (1) mitochondrial alterations as shown in fig 5 (2) antioxidant effects (fig 4) and (3) effects on cancer progression such as the 2-DG (fig 6). Based on these data, introduce the proteomics experiment. Then show the proteomics data and validation experiments. Explain the pathways differentially regulated in the proteomics experiment and explain why UCP2 knockdown causes these metabolic effects.*

**Response:** We thank the Reviewer for giving us the opportunity to re-organize the chronological order of our data and to improve our manuscript. We followed the indications of the Reviewer starting from the simplest data. Indeed, we have first shown experiments concerning the antioxidant capacity and the mitochondrial alterations induced by UCP2 and the effects on the cellular sensitivity to 2-DG. Then, we introduced proteomics data and validation experiments. Finally, we showed the novel molecular insights associated to the glycolytic phenotype induced by UCP2 in

cancer cells. The old Fig.1 has been removed from the main figures and inserted as supplementary material.

*2. The need for the proteomics experiment is not clearly justified. Further, while reporting the results from the proteomics experiment, focus on the pathways of interest. Other proteins/pathways could be explained later. No need for detailed explanation of the pie chart.*

**Response:** In the revised version of our manuscript we introduced that proteomics experiments have been performed to investigate novel molecular insights related to the regulation of pancreatic cancer cell growth and metabolism by UCP2. As required by the Reviewer we focused on the proteomics results concerning proteins strictly involved in the pathway of interest, especially hnRNPA2/B1. The other proteins found modulated by genipin using the proteomics approach are commented in the discussion section. Pie chart description has been shortened, as well as the description of modulated proteins that are not apparently involved in the main pathway.

*3. Representative 2D gels from different experimental groups should be shown.*

**Response:** In the revised version of our manuscript we inserted representative 2D gels from untreated and genipin-treated experimental groups (Supplementary Figure 3).

*4. The immunohistochemistry data in figure 3C is not clear.*

**Response:** New figure 4 panel D has been inserted to facilitate the comprehension of the representative images showing the down-modulation of GLUT1 expressions in cancer cells exposed to genipin treatment.

*5. Is fig 5B, a western blot for individual subunits of different mitochondrial complexes? Then the names of the subunits need to be mentioned. It cannot be equated with the expression of the entire complex in the graphs.*

**Response:** As required by the Reviewer, in the legend of Figure 6 panel A we specified the name of the subunits of the various mitochondrial complexes analyzed.

*Minor:*

*1. When reporting the validation of proteomics data by western analysis, donot discuss the importance of the protein in the results section. This can be done in the discussion section.*

**Response:** Amended. We shifted this part in the discussion section.

*2. The differentially expressed proteins described in the results section need to be highlighted in a schematic or table to indicate the importance of the pathway or process of family of proteins. Otherwise the text in the results section will lose its focus.*

**Response:** Amended. We removed them from the results. The differentially expressed proteins found with proteomics profiling are summarized in Table 1 and functionally clustered in Supplementary Figure 4. A final model of our study is reported in Figure 7.

*3. The entire manuscript needs o be checked for grammatical mistakes and typographical errors. One example is as follows:*
*Page 4, para 2: sentence 1: Replace "to" with "with".*
*Sentence 2: Not clear. Please simplify and rephrase into smaller sentences.*

**Response:** Amended.

*Reviewer #4: Manuscript FRBM-D-16-00676 by Jessica Brandi et al reports an interesting, timely and well performed study on mechanistic aspects of the metabolic alterations in pancreatic cancer cells mediated by changes in UCP2 expression or activity. By means of a proteomic approach and complementary experiments, the authors provide convincing evidence that inhibition of UCP2 with genipin and/or downregulation of UCP2 expression with a specific siRNA inhibits expression of hnRNPA2/B1, the glucose transporter GLUT1 and the key glycolytic enzyme PKM2. These effects appear mediated by increased production of ROS upon inhibition of UCP2, and modulate the sensitivity of pancreatic cancer cells to the glycolytic inhibitor 2-deoxy-D-glucose.*
*The manuscript is well written, provides interesting mechanistic data and addresses an important aspect of metabolic switches in cancer cells, a hot topic in molecular oncology. The conclusions are well supported by the experimental evidence provided in the manuscript as well as by relevant controls presented as supplementary material. Accordingly, in its present form the manuscript would be of interest for FRBM readership. I have only a few minor suggestions for improvement, as follows.*

*1- The effects of inhibition of UCP2 with genipin or siRNA-mediated UCP2 downregulation on the expression of hnRNPA2/B1, GLUT1 and PKM2 are convincingly demonstrated at the protein level by a combination of proteomic analysis and Western blot. Although not absolutely required, it will be interesting to analyze the effects of such treatments on mRNA levels of the corresponding genes, to distinguish between transcriptional and post-transcriptional modes of regulation.*

**Response:** we thank the Reviewer for his/her comments/suggestions addressed to improve our manuscript. We performed qPCR analyses of hnRNPA2/B1, GLUT1 and PKM2 mRNAs after UCP2 inhibition with both genipin and siUCP2. New data are shown in new Figure 3 panel D and in new Figure 4 panel A. These new results indicate that hnRNPA2/B1, GLUT1 and PKM2

regulation by UCP2 occurs at the mRNA level. The effective knock-down of UCP2 by siUCP2 has been reported in Supplementary Figure 1A. Text has been modified accordingly.

*2- The analysis of overexpression of UCP2 on expression of hnRNPA2/B1, GLUT1 and PKM2 may also provide confirmatory support for the conclusions of the authors.*

**Response:** we analyzed the expression level of hnRNPA2/B1, GLUT1 and PKM2 genes by qPCR after overexpression of UCP2. In this condition we observed a marked up-regulation of all mRNAs tested (Figure 3D and 4A), thus further confirming the conclusions stated in UCP2 KD conditions. The effective overexpression of UCP2 has been reported in Supplementary Figure 1B. Text has been modified accordingly.

*3- Data on glucose consumption in the different relevant experimental conditions, again not absolutely required, might further strengthen the manuscript.*

**Response:** We agree with the Reviewer's comment. To further highlight the role of UCP2 on the glycolytic phenotype of cancer cells, we inserted a recent reference (Cho et al., Nuclear Medicine and Biology. Vol 43, Issue 10, Oct 2016, 587–592) describing the involvement of UCP2 on glucose uptake in cancer cells. A further comment has been added in the first paragraph of the discussion section, which is dedicated to mention the results observed in previous studies about the contribution of UCP2 on the Warburg effect.

*4- The authors should comment on the paradoxical observation in Fig 4B, where similar effects on hnRNPA2/B1 and PKM2 levels are reported for genipin (which induces ROS production) and NAC (which blocks ROS actions).*

**Response:** Figure 5 (ex-Figure 4) reports that genipin reduced the expression level of hnRNPA2/B1 protein while NAC alone failed to significantly modify hnRNPA2/B1 expression. The combination genipin+NAC was able to recover hnRNPA2/B1 protein inhibition by genipin. This is consistent with our statement about the role of ROS on hnRNPA2/B1 inhibition by genipin.
Concerning PKM2, although genipin+NAC combination recovered PKM2 inhibition by genipin supporting the crucial role of ROS, we also observed that NAC alone, as well as genipin alone, significantly reduced PKM2 expression. As we now discuss in the Results section of the revised manuscript, our hypothesis to explain this paradoxical effect is that the alteration of the overall cellular redox status might alter PKM2 expression. In support of this speculation is the fact that ROS production is described to both inhibit (Zhu J et al. 2014. PLoS ONE 9(12): e113733) and induce (Li Q et al. 2014. Article ID 504953, dx.doi.org/10.1155/2014/504953) PKM2 expression. Here, we show that the balancing of the cellular redox status by NAC addition to genipin treatment determined a rescue of PKM2 expression inhibited by genipin.

*5- The authoritative and recent review by Vyas, Zaganjor and Haigis (Cell 166, July 28 2016, 555-566) should be cited in the Introduction.*

**Response:** The reference indicated by the Reviewer has been inserted and commented in the Introduction of the manuscript.

**Dipartimento di Neuroscienze, Biomedicina e Movimento**
Piazzale Ludovico Antonio Scuro, 10 – 37134 VERONA – Policlinico "G.B. Rossi" | T +39 045 8124287
P. IVA 01541040232 | C.F. 93009870234

## Highlights

1. Proteomic profiling reveals several metabolic proteins/enzymes regulated by UCP2
2. UCP2 induces hnRNPA2/B1 through its antioxidant function in pancreatic cancer cells
3. UCP2 stimulates the expression of GLUT1, PKM2 and the secretion of L-lactic acid
4. UCP2 counteracts pancreatic cancer mitochondrial respiration and OXPHOS
5. UCP2 sensitizes pancreatic cancer cells to the glycolytic inhibitor 2-deoxy-D-glucose

# The antioxidant uncoupling protein 2 stimulates hnRNPA2/B1, GLUT1 and PKM2 expression and sensitizes pancreas cancer cells to glycolysis inhibition

Jessica Brandi[1*], Daniela Cecconi[1*], Marco Cordani[2*], Margalida Torrens-Mas[3], Raffaella Pacchiana[2], Elisa Dalla Pozza[2], Giovanna Butera[2], Marcello Manfredi[4,5], Emilio Marengo[4], Jordi Oliver[3], Pilar Roca[3], Ilaria Dando[2#], Massimo Donadelli[2#].

[1]*Department of Biotechnology, Proteomics and Mass Spectrometry Laboratory, University of Verona, Verona, Italy;*

[2]*Department of Neuroscience, Biomedicine and Movement, Biochemistry Section, University of Verona, Verona, Italy;*

[3]*Multidisciplinar Group of Translational Oncology, University Research Institute on Health Sciences (IUNICS), University of the Balearic Islands, E07122, Palma, Spain; Palma Institute for Health Research (IdISPa), E07010 Palma, Spain; Physiopathology of Obesity and Nutrition, CIBERobn (CB06/03), Carlos III Health Research Institute (ISCIII), Madrid, Spain;*

[4]*Department of Sciences and Technological Innovation, University of Eastern Piedmont, Alessandria, Italy;*

[5]*ISALIT, Novara, Italy.*

* *These authors equally contributed and share the first authorship*.

**[#]Corresponding authors:**

Massimo Donadelli, PhD. Department of Neuroscience, Biomedicine and Movement. Biochemistry Section, University of Verona, Verona, Italy. Strada Le Grazie 8, 37134 Verona, Italy.

phone: +39 045 8027281; fax: +39 045 8027170; e-mail: massimo.donadelli@univr.it

Ilaria Dando, PhD. Department of Neuroscience, Biomedicine and Movement. Biochemistry Section, University of Verona, Verona, Italy. Strada Le Grazie 8, 37134 Verona, Italy.

phone: +39 045 8027174; fax: +39 045 8027170; e-mail: ilaria.dando@univr.it

*Running title:* UCP2 sensitizes cancer cells to 2-DG

*Keywords:* cancer, metabolism, uncoupling proteins, UCP2, Warburg effect, proteomics.

**Abstract**

Several evidence indicate that metabolic alterations play a pivotal role in cancer development. Here, we report that the mitochondrial uncoupling protein 2 (UCP2) sustains the metabolic shift from mitochondrial oxidative phosphorylation (mtOXPHOS) to glycolysis in pancreas cancer cells. Indeed, we show that UCP2 sensitizes pancreas cancer cells to the treatment with the glycolytic inhibitor 2-deoxy-D-glucose. Through a bidimensional electrophoresis analysis, we identify 19 protein species differentially expressed after treatment with the UCP2 inhibitor genipin and, by bioinformatic analyses, we show that these proteins are mainly involved in metabolic processes. In particular, we demonstrate that the antioxidant UCP2 induces the expression of hnRNPA2/B1, which is involved in the regulation of both GLUT1 and PKM2 mRNAs, and of lactate dehydrogenase (LDH) increasing the secretion of L-lactic acid. We further demonstrate that the radical scavenger *N*-acetyl-$_{L}$-cysteine reverts hnRNPA2/B1 and PKM2 inhibition by genipin indicating a role for reactive oxygen species in the metabolic reprogramming of cancer cells mediated by UCP2. We also observe an UCP2-dependent decrease in mtOXPHOS complex I (NADH dehydrogenase), complex IV (cytochrome c oxidase), complex V (ATPase) and in mitochondrial oxygen consumption, suggesting a role for UCP2 in the counteraction of pancreatic cancer cellular respiration. All these results reveal novel mechanisms through which UCP2 promotes cancer cell proliferation with the concomitant metabolic shift from mtOXPHOS to the glycolytic pathway.

## 1. Introduction

Uncoupling proteins (UCPs) are mitochondrial anion transporter proteins localized into the mitochondrial inner membrane [1]. Currently, five UCP family members have been identified in mammals. Among them, UCP1 is highly expressed in brown adipose tissue playing a key role in adaptive non-shivering thermogenesis [2]. UCP2 (59% of amino acid sequence in common with UCP1) is widely distributed throughout the organism, suggesting different and wide functions for this mitochondrial uncoupling protein [3]. As a result of its ubiquitous distribution, UCP2 has been indicated to participate in several metabolic processes [4] and its misregulation is linked with the development of several diseases, including cancer [5, 6]. UCP3 is most abundantly expressed in skeletal muscle and, to a lesser extent, in brown adipose tissue and heart, and might play important roles in attenuation of reactive oxygen species (ROS) production and fatty acid metabolism [7]. Both UCP4 and UCP5 uncoupling family members are likely involved in the protection of neurons from an excessive production of ROS. They are primarily expressed in the central nervous system with marked dissimilarities in the expression level in different areas of the brain [8].

Among the various physio-pathological functions of UCP family members, the role of UCP2 in cancer has been recently recognized and attracted more attention. Many studies have well established the key role that UCP2 has in both tumorigenesis and chemoresistance. The generally accepted suggestion envisages that, during the first stages of tumorigenesis, UCP2 is down-regulated likely to allow ROS increase and genomic instability [6, 9], while it is triggered or over-expressed in the following stages of cancer development, finally determining resistance of cancer cells to therapies and tumor aggressiveness mainly through anti-apoptotic mechanisms induced by the attenuation of mitochondrial ROS production. This last item has been widely demonstrated in several cancer types, including pancreatic adenocarcinoma [10], breast cancer [11], leukemia cells [12], and drug-resistant colon cancer cells [13]. The antioxidant effect of UCP2 is mainly due by the transport of protons from the intermembrane space to the mitochondrial matrix bypassing ATP synthase. This event results in a decrease of several consequential events, as mitochondrial inner

membrane potential, electron leakage from respiratory electron transport chain and superoxide ion generation into mitochondrial matrix. Therefore, mild uncoupling of mitochondrial oxidative phosphorylation (mtOXPHOS) may represent the first line of defense against oxidative stress in cancer cells by decreasing mitochondrial respiration [14, 15]. Overall, since mitochondria are crucial organelles that can allow cancer cells to adapt to environmental alterations they are considered important mediators of tumor progression [16].

In the present study, we further investigated the involvement of mitochondrial UCP2 in biological and, especially, metabolic processes associated with pancreatic cancer cell proliferation. Overall, by using a proteomic approach we demonstrated that UCP2 regulates a number of crucial metabolic enzymes/proteins. In particular, we proved that UCP2 triggers the expression of: i) the heterogeneous nuclear ribonucleoprotein A2/B1 (hnRNPA2/B1); ii) the glucose transporter GLUT1; iii) the pyruvate kinase isoform M2 (PKM2); and iv) the lactate dehydrogenase (LDH) resulting in enhanced secretion of L-lactic acid. Overall these findings suggest that UCP2 promotes the glycolytic phenotype, thus determining an enhancement of cancer cell sensitivity to the glycolysis inhibitor 2-deoxy-D-glucose (2-DG). Furthermore, we observed that UCP2 reduces mitochondrial oxygen consumption and mtOXPHOS functionality without altering the overall amount of mtDNA. Finally, our results sustain the role of UCP2 as a crucial mediator in cancer cellular bioenergetic shift from mtOXPHOS to the glycolytic pathway.

## 2. Material and Methods

### *2.1 Chemicals*

Genipin (methyl-2-hydroxy-9-hydroxymethyl-3-oxabicyclonona-4,8-diene-5-carboxylate) and 2-deoxy-D-glucose (2-DG) were obtained from Sigma (Milan, Italy), solubilized in DMSO and bi-distillated sterile water, respectively, and stored at -80 °C until use. *N*-acetyl-$_L$-cysteine (NAC) was obtained from Sigma and solubilized in bi-distillated sterile water.

### *2.2 Cell culture*

Human pancreatic adenocarcinoma cell lines PaCa44 and Panc1 were grown in RPMI medium (Life Technologies, Milan, Italy), supplemented with 10% FBS, and 50 μg/ml gentamicin sulfate (BioWhittaker, Lonza, Bergamo, Italy). Cell lines were incubated at 37 °C with 5% $CO_2$.

### *2.3 Cell proliferation assay*

Cells were seeded in 96-well plates ($5\times10^3$ cells/well) and the day after were incubated with various compounds at the indicated conditions or transfected with the indicated constructs (see figure legends). At the end of the treatments, cell growth was measured by Crystal Violet assay (Sigma, Milan, Italy) according to the manufacturer's protocol, and absorbance was measured by spectrophotometric analysis ($A_{595}$nm).

### *2.4 Transient transfection assays*

Exponentially growing cells were seeded at a density of $5\times10^3$ cells/well in 96-well plates for proliferation assays and at $2.5x10^5$ cells/plate in 60 mm cell culture plates for protein extraction. The ectopic over-expression of UCP2 in cancer cells was carried out transfecting for 48 h the pCMV expression vector containing the human cDNA of UCP2 (OriGene Technologies, Rockville, MD) using Lipofectamine 3000 transfection reagent according to the manufacturer's instructions

(Thermo Fisher, Milan, Italy). Cells transfected with the pCMV empty vector were used as negative control (mock). Knock-down of UCP2 expression was obtained by transfecting cells with a specific small interfering (si) (5'-GCUAAAGUCCGGUUACAGATT-3') RNA targeting UCP2 mRNA and a non-targeting siRNA (5'-CAGUCGCGUUUGCGACUGG-3') used as negative control purchased by Ambion (Monza MB, Italy). Cells were transfected with siRNAs at a final concentration of 50 nM using Lipofectamine 3000 transfection reagent for 48 h (Thermo Fisher, Milan, Italy).

*2.5 RNA extraction and qPCR*

Total RNA was extracted from $10^6$ cells using TRIzol Reagent (Life Technologies, Milan, Italy), and 1 μg of RNA was reverse transcribed using first-strand cDNA synthesis. Real-time quantification was performed in triplicate samples by SYBR Green detection chemistry with Power SYBR Green PCR Master Mix (Applied Biosystems) on a 7000 Sequence Detection System. The primers used were: Hs_UCP2_1_SG QuantiTect Primer Assay (Qiagen, Milan, Italy) for the UCP2 gene; hnRNPA2/B1 F: 5'-AGC TTT GAA ACC ACA GAA GAA-3', hnRNPA2/B1 R: 5'-TTG ATC TTT TGC TTG CAG GA-3'; GLUT1 F: 5'-CAT CAT CTT CAT CCC GGC-3', GLUT1 R: 5'-CTC CTC GTT GCG GTT GAT-3'; PKM2 F: 5'-CAG AGG CTG CCA TCT ACC AC-3', PKM2 R: 5'-CCA GAC TTG GTG AGG ACG AT-3'; and Hs_RRN18S_1_SG QuantiTect Primer Assay for 18S rRNA. The thermal cycle reaction was performed as follows: 95 °C for 10 minutes followed by 40 cycles at 95 °C for 15 seconds and 60°C for 1 minute. Three independent experiments were performed for each assay condition.

*2.6 2DE proteomics analysis*

2DE protein analysis from $1.5x10^6$ PaCa44 cells, untreated and treated with 150 μM genipin for 16 h, was performed as previously described [17]. Briefly, 500 μg of protein were subjected to IEF with 17 cm immobilized nonlinear pH 3–10 gradient IPG strips using a Protean IEF Cell (Bio-

Rad). After IEF, IPG strips were equilibrated and then the proteins were separated using 8–18% SDS-PAGE gels. Ruthenium chelate (RuBPs) fluorescent staining was used to visualize protein spots on 2DE gel. The protein pattern differential analysis of 10 stained gels (5 technical replicates x 2 samples, i.e. control and genipin treated cells) were performed by PDQuest software v7.3 (Bio-Rad).

*2.7 Protein identification by nano-HPLC-Chip ion trap MS/MS*

Protein identification was performed after in-gel trypsin digestion, as previously described [17]. Briefly, peptides from each sample were separated by RP nano-HPLC-Chip technology (Agilent Technologies, Palo Alto, CA, USA) online-coupled with a 3D ion trap mass spectrometer (model Esquire 6000, Bruker Daltonics, Bremen, Germany). Database searches were conducted using the MS/MS ion search of Mascot against human entries of the non-redundant NCBI database.

*2.8 Protein annotation and enriched pathways analysis*

Functional annotation of identified proteins was performed according to Gene Ontology (GO) using the PANTHER classification system v 9.0 (http://www.pantherdb.org/) according to biological processes, molecular functions and cellular components. Enrichment pathways analysis was done using STRING 9.1 database (http://string-db.org). Gene Ontology terms and enriched pathways were considered significant for adjusted p-values lower than 0.05.

*2.9 Immunoblot analysis*

Cells were harvested, washed in PBS, and re-suspended in lysis buffer in the presence of phosphatase and protease inhibitors (50 mM Tris–HCl pH 8, 150 mM NaCl, 1% Igepal CA-630, 0.5% Na-Doc, 0.1% SDS, 1 mM $Na_3VO_4$, 1 mM NaF, 2.5 mM EDTA, 1 mM PMSF, and 1× protease inhibitor cocktail). After incubation on ice for 30 min, the lysates were centrifuged at 14,000 × g for 10 min at 4 °C and the supernatant fractions were used for Western blot analysis.

Protein concentration was measured by Bradford reagent (Pierce, Milan, Italy) using bovine serum albumin as a standard. Protein extracts (50 μg/lane) were resolved on a 12% SDS-polyacrylamide gel and electro-blotted onto PVDF membranes (Millipore, Milan, Italy). Membranes were blocked in 5% low-fat milk in TBST (50 mM Tris pH 7.5, 0.9% NaCl, 0.1% Tween 20) for 1 h at room temperature and probed overnight at 4 °C with goat polyclonal anti-UCP2 (1:1000) (Abnova), rabbit anti-GLUT1 (1:1,000) (Abcam, #ab652), rabbit polyclonal anti-phospho-(Tyr105)PKM2 (1:1,000) (Cell Signaling #3827), mouse polyclonal anti-PKM2 (1:1,000) (Sigma # WH0005315M1), mouse anti-hnRNPA2/B1 (1:400) (Santa Cruz sc-374053), rabbit anti-stathmin 1 (1:5,000) (Sigma Aldrich O-01238), antisera against mtOXPHOS complexes (MitoSciences, OR, USA), or rabbit monoclonal glyceraldehyde 3-phosphate dehydrogenase (GAPDH) (1:1,000) (Cell Signaling, #5174S) antibodies. Horseradish peroxidase conjugated anti-mouse, anti-goat or anti-rabbit IgGs (1:8,000 in blocking solution) (Upstate Biotechnology, Milan, Italy) were used as secondary antibodies. Immunodetection was carried out using chemiluminescent substrates and recorded using a HyperfilmECL (Amersham Pharmacia Biotech). ECL results were scanned and the amount of each protein band quantitated using NIH Image J software (http://rsb.info.nih.gov/nih-image/).

*2.10 L-lactic acid quantification in culture medium*

After the transfection period, culture medium has been taken and diluted 30-fold in $H_2O$. For each sample 25 μl has been analyzed in a final reaction volume of 500 μl (Megazyme, #K-LATE 07/14). Absorbance at 340 nm has been read after 10 minutes the activation of the reaction and L-lactic acid concentration (g/L) has been calculated according to the manufacturer's instructions.

*2.11 Measurement of mitochondrial superoxide production*

The non-fluorescent MitoSox Red probe (Molecular Probes, Thermo Fisher, Milan, Italy) was used to evaluate mitochondrial $O_2$•− production as described in [18]. Briefly, cells were seeded

in 96-well plates ($5\times10^3$ cells/well) and, the day after, treated with 150 µM genipin for 16 h. At the end of treatment, cells were incubated in culture medium with 0.5 µM MitoSox probe at 37 °C for 15 min. Cells were washed with Hanks buffer (20 mM Hepes pH 7.2, 10 mM glucose, 118 mM NaCl, 4.6 mM KCl, and 1 mM $CaCl_2$) and fluorescence was measured by using a multimode plate reader (Ex 430 nm and Em 590 nm) (GENios Pro, Tecan, Milan, Italy). The probe is live-cell permeant and is rapidly and selectively targeted to the mitochondria where it becomes fluorescent after oxidation by $O_2$•−. The usage of 430±35 nm of excitation wavelengths allowed us to selectively detect mitochondrial $O_2$•− strongly reducing the recognition of other oxidants (e.g., •OH, ONOO•−) [19, 20]. The values were normalized on cell proliferation by Crystal Violet assay.

*2.12 Immunofluorescence (IF) and Laser Confocal Microscopy (LCM)*

PaCa44 cells treated or untreated with genipin were fixed in 4% paraformaldehyde (PFA; 15 min) and, after 4 changes (10 min each) of PBS, were permeabilized in 0.1% Triton X–100 (5 min) in PBS. To saturate unspecific binding sites, the cells were incubated for 45 min at room temperature (RT) with a blocking solution containing 5% BSA and 0.05% Triton X-100 in PBS. Samples were then incubated overnight at 4 °C with anti-GLUT1 (1:500) (from Abcam, Cambridge, UK) primary antibody diluted in blocking solution. After 3 washes with PBS (10 min each), cells were incubated for 1h at RT in the dark with specific secondary antibodies (1µg/mL) conjugated with Alexa Fluor-488 (Molecular Probes, Invitrogen Corporation, Carlsbad, CA). The incubation with secondary antibodies was followed by a 10 min incubation with 1.0 µg/mL of 4′, 6-diamidino-2-phenylindole dihydrochloride (DAPI, Sigma). Coverslips were mounted in anti-bleaching medium (Dako Fluorescent Mounting Medium, Dako, CA, USA). The negative control procedure omitted the primary antibody.

LCM acquisition was performed using a Leica TCS SP5 AOBS microscope (Leica–Microsystems, Wezlar, Germany) equipped with violet (405 nm laser diode), blue (argon, 488 nm), orange (543 nm) and red (633 nm, HeNe laser) excitation laser lines. A 63x / 1.40 NA oil-

immersion objective (HCX PL APO 63x 1.40 OIL UV, Leica-Microsystem) was employed for the analysis. The acquisition conditions were set to prevent fluorescence loss and to cause minimal photo-damage. All images were acquired with the following sequential settings: zoom 2.0; format 2048 x 2048; pixel size 0.120 x 0.120 µm and pinhole was set to 1.0 Airy unit.

*2.13 Mitochondrial membrane potential (ΔΨm)*

Mitochondrial membrane potential was measured fluorimetrically by using tetramethylrhodamine methyl ester (TMRM) probe. PaCa44 cells were seeded in 96-well plates ($7x10^3$ cells/well) and treated with 150 µM genipin for 16 h or transfected with siRNA-UCP2 for 48 h. After treatment, cells were exposed to 100 nM TMRM for 15 min and fluorescence measurement was performed in an FLx800 microplate fluorescence reader (Bio-Tek Winooski, VT, USA) set at excitation and emission wavelengths of 552 and 576 nm. Values were normalized per number of viable cells determined by crystal violet assay.

*2.14 Enzymatic activities*

Cells were harvested 48h after transfection by scraping them into 200 µl of STE buffer (250 mM sucrose, 3.59 mM Trizma-Base, 16.4 Tris-HCl pH 7.4, 2 mM EDTA, 40 mM KCl). Then, cells were disrupted by sonication at 40% amplitude for 10 seconds three times (VibraCell 75185) and centrifuged at 600 × g for 10 min at 4 °C to remove cell debris. Protein content (supernatant) was determined with a bicinchoninic acid (BCA) protein assay kit (Pierce, Bonn, Germany) and the enzymatic assays were performed immediately after.

Cytochrome c oxidase (COV, Complex IV, EC 1.9.3.1) activity was measured using a spectrophotometric assay. Briefly, cell lysate was incubated in 0.1 M $NaPO_4H_2$, pH 7.0 in the presence of 2 µg/mL catalase and 5 mM substrate DAB (3,3'-diaminebenzidine-tetrachloride) and then 100 µM of reduced cytochrome c was added to start the reaction. The absorbance increment

was followed for 25 min at 450 nm and 37 °C. The generated slope is directly proportional to the activity of COX.

ATP synthase (ATPase, ATP phosphohydrolase, Complex V, EC 3.6.1.3) activity was measured by following the oxidation of NADH at 340 nm and 37 °C. Briefly, cell lysate was incubated in assay buffer (0.33 M sucrose, 6.3 mM $MgSO_4$, 63.66 mM HEPES, 0.442 mM NADH, pH 8.0) in the presence of 2.5 mM Phospho(enol)pyruvic acid, 0.5 µg/mL Pyruvate Kinase, 0.25 µg/mL l-Lactic dehydrogenase and 0.1 µg/mL antimycin. Then, 5 mM ATP was added to start the reaction. The extinction coefficient used was 6.22 $mM^{-1}cm^{-1}$. The absorbance reduction was followed for 15 min and the maximum slope was taken to analyze activity data. The generated slope is inversely proportional to the activity of ATPase.

*2.15 mtDNA quantification*

DNA was isolated from cultured cells using the innuPREP DNA Mini Kit (Analytik Jena) following the manufacture protocol. The extracted DNA was quantified using a spectrophotometer (BioSpec-nano) to amplify 5 ng of DNA using specific primers for 18S and the NADH dehydrogenase subunit 4 (mitochondrial) with SYBR Green Technology on a LightCycler 480 System II (Roche Diagnostics, Basel, Switzerland). Total reaction volume was 10 µL, containing 7.5 µL Lightcycler® 480 SYBR Green I Master, 0.5 µM of the sense and antisense specific primers and 2.5 µL of the DNA. The thermal cycle reaction was performed as follows: 95 °C for 5 minutes followed by 45 cycles at 95 °C for 10 seconds and 60 °C for 10 seconds, and an extension step at 72 °C for 12 seconds. A negative control without cDNA template was run for each gene. The primers used were forward 5'-GGA CAC GGA CAG GAT TGA CA-3' and reverse 5'-ACC CAC GGA ATC GAG AAA GA-3' for 18S, and forward 5'-CGT GAC TCC TAC CCC TCA CA-3' and reverse 5'-ATC GGG TGA TGA TAG CCA AG- 3' for the NADH dehydrogenase subunit 4 (mtDNA) .The Ct values of the real-time PCR were analysed, referring these results to the total DNA amount, using the GenEx Standard Software (MultiDAnalises, Sweden).

*2.16 Oxygen consumption rate*

After transfection, cells were harvested and 1.25 x $10^6$ cells were incubated in 0.5 mL of DMEM in a water-thermostatically regulated chamber with a computer-controlled Clark-type $O_2$ electrode (Oxygraph; Hansatech, Norfolk, UK). Cells were preincubated for 5 min at 37 °C and basal respiration rate was measured. Next, 1 µM oligomycin was added to the chamber to reveal ATP synthase-dependent oxygen consumption. Then, 8 µM FCCP was added to observe maximal respiration and finally 1 µM antimycin was added to inhibit the electron transport chain and stop mitochondrial oxygen consumption. Each oxygen consumption rate was measured three times during 7 min.

*2.17 Statistical analyses*

ANOVA (post hoc Bonferroni) analysis was performed by GraphPad Prism 5 software. p values < 0.05 and 0.01 were indicated as (*) or (**), respectively. In 2-DE image analysis, Student's t test ($p < 0.05$) was applied on log-transformed protein volumes normalized by intensities of all valid spots using PDQuest (Bio-Rad). Multivariate statistics of 2DE image analysis was performed with Simca-P+ v12.0 (Umetrics, Sweden). In particular for identification of proteins separating control from genipin-treated cells, we used orthogonal partial least squares discriminant analysis (OPLS-DA), applying a variable influence on projection (VIP) >1.5 to identify the protein spots that contributed most to the calculated OPLS-DA model. We only considered protein spots that showed good correlations [p(corr)>0.7] by the multivariate OPLS-DA and that differed from controls with significances better than $p<0.05$ by using the Student's t test.

## 3. Results

### *3.1 The antioxidant mitochondrial uncoupling protein UCP2 sensitizes pancreatic cancer cells to the glycolytic inhibitor 2-DG*

To investigate novel molecular mechanisms and metabolic alterations driven by UCP2 in pancreatic cancer cells we overexpressed or down-regulated UCP2 expression using transient transfection tools described in Material and Methods section. Furthermore, we also used genipin, a pharmacological inhibitor of UCP2 activity, to confirm some crucial results obtained in the present study. We first aimed to confirm the selective effect of genipin on UCP2 inhibition analyzing the outcome of this drug in pancreatic cancer cell growth in UCP2-deficient conditions. **Figure 1A** shows that UCP2 knockdown by a specific siRNA-UCP2 significantly reduced the antiproliferative effect of genipin in PaCa44 cells. In addition, genipin was able to increase mitochondrial superoxide production and mitochondrial membrane potential in pancreatic cancer cells. Indeed, genipin increased both the mitochondrial superoxide level in PaCa44 cells (~20-folds) (**Figure 1B**) and the proton gradient in the inner mitochondrial membrane (71%), as did the siUCP2 (41%) (**Figure 1C**). Altogether these data support the specific effect of genipin on the inhibition of the antioxidant mitochondrial uncoupling protein UCP2 in our experimental system.

Since UCP2 has been previously described to support the glycolytic phenotype [21, 22], we here aimed to analyze whether the sensitivity of pancreatic cancer cells to glycolysis inhibitors might be influenced by UCP2 expression. In order to achieve this purpose we evaluated the response of pancreatic cancer cells to 2-deoxy-D-glucose (2-DG), a stable glucose analogue widely used as a glycolytic flux inhibitor, after knockdown or overexpression of UCP2. The effective modulation of UCP2 expression by transfection tools has been confirmed with qPCR experiments (**Supplementary Figure 1**). Our data show that the transient knockdown of UCP2 significantly decreased the sensitivity of PaCa44 cells to 2-DG if compared to its negative control (**Figure 2A**), while, UCP2 overexpression conferred a strong sensitization to 2-DG incubation, as compared to its

relative mock vector (**Figure 2B**). Similar results were obtained in another pancreatic cancer cell line, Panc1 cells (**Supplementary Figure 2**). Overall, these results demonstrated that the oncogenic properties of UCP2 might be specifically counteracted by targeting glycolysis, thus representing a novel and effective therapeutic strategy for pancreas cancer patients having high UCP2 expression levels.

*3.2 Bidimensional proteomic profiling of pancreatic cancer cells treated with the UCP2 inhibitor genipin*

To unravel novel molecular insights related to the regulation of pancreatic cancer cell growth and metabolism by UCP2 we performed a bidimensional proteomic profiling of PaCa44 cells treated with genipin. **Supplementary Figure 3** shows representative 2D gels from untreated and genipin-treated cells. About 500 polypeptide spots were revealed in the pH 3-10 interval with the high-sensitivity RuBPs stain, and then matched between the different gels. To quantify level changes of individual spots and also to detect interrelationships between them and thereby explore categories of differential protein expression, the normalized spot volumes were subjected to both univariate and multivariate statistics analysis. The criteria used for protein identification choice with a difference greater than 30%, with $p< 0.05$ by Student's *t* test, and/or with p(corr)>0.7 by the multivariate OPLS-DA, yielded 24 apparent protein spots. All these modulated spots were successfully picked up and a total of 19 protein species were identified by nano-HPLC-Chip ion trap MS/MS and detailed in **Table 1**. By bioinformatic analyses, we found that the cellular components mostly over-represented in genipin-treated cells were extracellular exosome (28%), extracellular membrane-bounded organelle (17%), membrane-bounded organelle (17%) and cytosol (17%). In addition, the GO enrichment analysis suggests that the identified proteins are mainly involved in metabolic process (31%), cellular process (18%) and component organization (13%), as well as developmental process (13%). As concerning the molecular function category, we found

among the most prominent significant GO enriched terms the catalytic activity (59%), binding (17%), and structural molecule activity (12%) (**Supplementary Figure 4**).

Among the 19 identified protein species by 2DE analysis reported in Table 1 some are related with the promotion of cancer cell proliferation by UCP2, in accordance with our previous discoveries [10, 15]. Indeed, the expression of one form of stathmin 1 is decreased 1.37 fold in PaCa44 cells treated with genipin in comparison to untreated cells (Table 1). Furthermore, this result has been validated by 1D-WB in PaCa44 cells treated with genipin showing a decreased expression of stathmin 1 in comparison to control cells (**Figure 3A**). Stathmin 1 has been proposed as a potential prognostic marker for patients with non-small cell lung cancer [23] and has been shown to lead resistance to chemotherapeutic agents in human esophageal squamous cancer cells [24], whose overexpression prevented TGFβ-mediated growth inhibition of pancreatic cancer cells [25], suggesting a role for stathmin 1 in the UCP2-mediated chemoresistance of pancreas cancer cells.

Interestingly, the protein hnRNPA2/B1, a known regulator of the alternative splicing of the glycolytic enzyme pyruvate kinase (PK) [26], is strongly repressed (<20 fold) by genipin in PaCa44 cells (Table 1). Thus, we also validated by 1D-WB the protein hnRNPA2/B1, whose expression strongly decreased in PaCa44 cells treated with genipin in comparison to control cells (**Figure 3B**). Furthermore, 2DE-WB analysis of hnRNPA2/B1 revealed six signals in untreated cells at pI from ~7 to ~9 and the most basic protein isoform appears to be present only in untreated cells, while it is absent in cells treated with genipin (**Figure 3C**), in accordance with the proteomic data (Table 1). The qPCR approach further revealed that UCP2 inhibition by genipin or siUCP2 significantly repressed hnRNPA2/B1 mRNA expression, while UCP2 overexpression enhanced its mRNA level, strongly suggesting a transcriptional regulation of hnRNPA2/B1 gene driven by UCP2 (**Figure 3D**).

*3.3 UCP2 stimulates GLUT1 and PKM2 expression in pancreatic cancer cells*

Since hnRNPA2 family members have been found to bind and regulate GLUT1 mRNA expression in cancer cells [27] and the alternative splicing of the pyruvate kinase isoform M2 (PKM2) by including the exon 10 in the mRNA [26], we investigated whether UCP2 might trigger the up-regulation of both GLUT1 and PKM2 expression, in addition to the induction of hnRNPA2/B1. Accordingly, we demonstrated that UCP2 inhibition by genipin or siUCP2 significantly repressed both GLUT1 and PKM2 mRNA expression levels, while UCP2 overexpression enhanced their mRNA levels (**Figure 4A**). These data were further confirmed at the protein level by Western blot assay. Indeed, both GLUT1 and PKM2 protein expression levels were down-modulated after treatment with genipin (**Figure 4B**) or siUCP2 (**Figure 4C**). We further observed a marked reduction of GLUT1 expression in genipin-treated cells as compared to control cells by using confocal microscopy immunofluorescence (**Figure 4D**), thus confirming the involvement of UCP2 in the up-regulation of GLUT1 in pancreatic cancer cells. Finally, the quantification of the L-lactic acid in the cell culture medium showed that UCP2 over-expression significantly increased the secretion of L-lactic acid in comparison to negative control (**Figure 4E**), thus supporting the stimulation of the glycolytic phenotype by UCP2 in pancreatic cancer cells and the enhancement of the UCP2-related sensitivity of these cells to the glycolytic inhibitor 2-DG (Figure 2).

*3.4 The antioxidant function of UCP2 is involved in hnRNPA2/B1 and PKM2 stimulation*

To further investigate the bases of the metabolic modifications driven by UCP2 we analyzed whether the antioxidant function of UCP2 might have a role in the stimulation of hnRNPA2/B1 and PKM2. First, we confirmed that UCP2-inhibition by genipin was able to induce mitochondrial ROS production in these cells (Figure 1B). Furthermore, the addition of the radical scavenger *N*-acetyl-$_{L}$-cysteine (NAC), previously described by our group to be able to revert the antiproliferative effects induced by genipin in these cells [15], strongly rescued both hnRNPA2/B1 and PKM2 expression inhibition by genipin (**Figure 5**). The observed down-modulation of PKM2 expression by both the

pro-oxidant agent genipin and the antioxidant NAC alone might be explained by previous data reporting that the alteration of the overall cellular redox status might modify PKM2 expression [28, 29]. Altogether these results suggest that the glycolytic pathway triggered by UCP2 in pancreatic cancer cells might be mainly assured by its antioxidant function.

*3.5 UCP2 counteracts pancreatic cancer cellular respiration inhibiting mtOXPHOS and oxygen consumption*

To further evaluate the effects of UCP2 on mitochondrial metabolism, we also performed different analyses on OXPHOS mitochondrial complexes and oxygen consumption rate. We observed a general increase in all OXPHOS complexes with siUCP2, which resulted significant for the subunit NDUFB8 of the complex I (NADH dehydrogenase), the subunit COX II of the complex IV (cytochrome c oxidase) and the subunit ATP5A of the complex V (ATPase), as shown in **Figure 6A**. Furthermore, both enzymatic activities of complex IV and complex V significantly increased by 27% and 25%, respectively, when UCP2 was knocked-down (**Figure 6B** and **6C**). On the other hand, we evaluated the mitochondrial DNA (mtDNA) content to check whether there was an increase in the overall amount of mitochondria after UCP2 inhibition. As shown in **Figure 6D**, cells transfected with siUCP2 did not show any changes in mtDNA copy number. As shown in **Figure 6E** and **Supplementary Figure 5** basal oxygen consumption rate (OCR) was significantly higher in UCP2-knockdown cells compared to control ones. The difference between basal rate and rate after oligomycin addition corresponds to the oxygen consumed for ATP production, which is higher in siUCP2 transfected cells. The mitochondrial uncoupler FCCP and antimycin were sequentially added to evaluate maximal cellular respiration. Finally, maximal respiration, calculated as the difference between the rate after FCCP addition and the rate after antimycin addition, was also greater in cells with UCP2 knockdown (Figure 6E).

**4. Discussion**

Nowadays, the study of the metabolic aberrations in cancer disease is very intense and debated since they might represent a therapeutic target to selectively inhibit neoplastic proliferation [30, 31]. In a recent article, Xu *et al.* stated that mitochondrial uncoupling mediated by UCPs leads the shift of cell metabolism from mtOXPHOS to aerobic glycolysis, also named Warburg effect, as a metabolic adaptation of cancer cells bearing antioxidant-deficient mitochondria [32]. Data presented by Xu *et al.* support the previous knowledge about UCP2 involvement in the maintenance of Warburg effect in cancer, as demonstrated by the high production of lactate after overexpression of uncoupling proteins [13]. Recently, Cho *et al.* demonstrated that genipin or siRNA-UCP2 strongly reduced the uptake of $^{18}$F-fluoro-deoxyglucose and consequently the secretion of lactate in breast and colon cancer cells [33].

In addition to the antioxidant property of UCP2 by allowing the flux of protons from the mitochondrial intermembrane space to the mitochondrial matrix [34], the channel formed by this protein can also promote the mitochondrial efflux of pyruvate and of Krebs cycle intermediates towards the cytosol, thus limiting the mitochondrial oxidation of glucose- and glutamine-derived metabolic intermediates [35]. Furthermore, Samudio *et al.* revealed that the exposure of leukemia cells to mesenchymal stromal cells results in increased accumulation of lactate in the culture medium, indicative of the Warburg effect. Most notably, the increased glycolytic phenotype is accompanied by decreased mitochondrial membrane potential in the leukemic cells as a result of mitochondrial uncoupling promoted by UCP2, suggesting that the Warburg effect mediated by uncoupling proteins might also be triggered by cancer-stroma crosstalk [36]. Accordingly, Zhang *et. al*. further demonstrated that during early differentiation human pluripotent stem cell proliferation slows, energy metabolism decreases, and UCP2 expression is repressed, resulting in decreased glycolysis and preserved or increased mitochondrial glucose oxidation [22]. Overall, these findings are in accordance with the observations that UCP2 is commonly over-expressed in neoplastic tissues, as breast, ovarian, leukemia, bladder, esophagus, testicular, colorectal, kidney, pancreatic,

lung and prostate cancers [21] and that the glycolytic pathway is generally strongly enhanced in cancer cells [37].

Our recent studies demonstrated that mitochondrial uncoupling mediated by UCP2 inhibits autophagic cell death making pancreatic cancer cells particularly resistant to the anticancer drug gemcitabine [10, 15]. In a previous study, we have also functionally associated this phenomenon with the UCP2-mediated cytosolic stabilization of the glycolytic enzyme glyceraldehyde-3-phosphate dehydrogenase (GAPDH). Indeed, we revealed that ROS produced by inhibition of UCP2 are able to stimulate the oxidation of GAPDH glycolytic enzyme determining conformational changes, which favor its translocation into the nucleus where it can subsequently trigger the expression of cell death- and autophagy-related genes [15]. Therefore, UCP2 can prevent the activation of autophagic genes and concurrently stabilize the glycolytic enzyme GAPDH in the cytosol where glycolysis takes place making mitochondrial uncoupling a functional crossroad between Warburg effect, autophagy and ROS regulation. By proteomic profiling we here report in Table 1 that the expression of one form of nucleophosmin, a protein that regulates the nuclear translocation of the glycolytic enzyme glyceraldehyde 3-phosphate dehydrogenase (GAPDH) [38], decreased 2.56 fold after genipin treatment, supporting our previous data that stated the enhancement of GAPDH nuclear translocation in pancreas cancer cells after UCP2 inhibition [15], further proving novel insights in the stimulation of the Warburg effect by UCP2. In this context, we provide here further evidence and novel insights, schematically reported and summarized in **Figure 7**, concerning the crucial role of UCP2 on the metabolic shift from mtOXPHOS to glycolysis in pancreas cancer cells. By using a bidimensional proteomic approach and gene ontology classifications [39] we observed that the differentially expressed proteins after UCP2 inhibition are mainly related to metabolic processes. In particular, we revealed that UCP2 induces expression of hnRNPA2/B1 through its antioxidant function, suggesting its involvement in the up-regulation of both GLUT1 and pyruvate kinase isoform M2 (PKM2) resulting in enhanced lactate secretion. In addition to GLUT1 and PKM2 stimulation, we also reported in Table 1 that a form of LDH, a key

enzyme involved in L-lactic acid fermentation, emerged to be strongly downregulated (<20 fold) after UCP2 inhibition by genipin, thus supporting a role of UCP2 in the maintenance of the glycolytic phenotype of cancer cells [31, 32].

On the other side, the metabolic shift from mtOXPHOS to glycolysis, and the consequent enhanced sensitivity of cancer cells to the glycolysis inhibitor 2-DG, are further revealed by the UCP2-mediated repression of OXPHOS complexes expression/activity and oxygen consumption. Interestingly, mtDNA amount remains unchanged suggesting that OXPHOS inhibition by UCP2 is not due to mitochondria amount alteration. Finally, manganese superoxide dismutase (MnSOD) was found to be downregulated (-1.53 fold) after genipin treatment (Table 1), suggesting its involvement in the UCP2-mediated metabolic shift towards glycolysis in cancer cells. Indeed, it has been recently demonstrated that MnSOD upregulation in cancer cells established a steady flow of $H_2O_2$ originating from mitochondria that sustains AMP-activated kinase (AMPK) activation and the metabolic shift to glycolysis, indicating that the MnSOD/AMPK axis is critical to support the Warburg effect [40]. Furthermore, porin-1 (VDAC1), enhanced 1.4 fold after genipin treatment (Table 1), has been demonstrated to strongly modulate mitochondrial metabolism of cancer cells, beyond its role on mitochondrial autophagy [41].

Altogether our findings provide novel mechanistic insights into the metabolic regulation driven by UCP2 and unveil the inhibition of glycolysis pathway as a strategic therapeutic approach against UCP2-overexpressing human cancers.

**Acknowledgements**

This work was supported by Joint Projects program 2015 from University of Verona to M. Donadelli (n. B12I15002320003); by grant from Fondo de Investigaciones Sanitarias of Instituto de Salud Carlos III (PI12/01827 and PI14/01434) of the Spanish Government confinanced by FEDER-Unión Europea ("Una manera de hacer Europa"). I. Dando is a fellow of Fondazione Umberto Veronesi. E. Dalla Pozza is a fellow of AIRC 5 per mille (grant no. 12182). M. Torrens-Mas is a fellow of Ministerio de Educación, Cultura y Deporte of Spanish Government (FPU grant).

**Conflict of interest**

The authors declare that they have no conflicts of interest.

**Legends to Figures**

**Figure 1.** Effect of UCP2 inhibition on cell growth, reactive oxygen species production and mitochondrial membrane potential in PaCa44 cells. (**A**) Cell growth was measured by using Crystal Violet colorimetric assay. Cells were seeded in 96-well plates, incubated overnight, and treated with 150 μM genipin for 16 h and/or transfected with siUCP2. (**B**) PaCa44 cells were seeded in 96-well plates, incubated overnight, and treated with 150 μM genipin for 16 h. The fluorescence intensity of the MitoSox Red probe, corresponding to the level of mitochondrial superoxide production, was measured by using a multimode plate reader, as described in Material and Methods. (**C**) Mitochondrial membrane potential ($\Delta\Psi m$) was measured fluorimetrically in PaCa44 cells treated with 150 μM genipin for 16 h or transfected with siUCP2 using TMRM, as described in Material and Methods. Values are the means ± SEM of three independent experiments each performed in triplicate. Statistical analysis: * $p<0.05$, ** $p< 0.01$, and *** $p<0.001$ genipin and/or siRNA UCP2 versus Ctrl, and genipin+siRNA UCP2 versus genipin.

**Figure 2.** UCP2 sensitizes PaCa44 cells to the treatment with the glycolytic inhibitor 2-deoxy-D-glucose (2-DG). Cells were seeded in 96-well plates and transfected for 48 h with siUCP2 or a nontargeting siRNA used as negative control (siCTRL) (**A**), or with the pCMV expression vector containing the human cDNA of UCP2 to overexpress UCP2 (o.e. UCP2) or with empty vector (mock) (**B**). For each experimental condition, cells were untreated or treated with 1, 2.5 or 5 μM 2-DG for 48 h. Cell growth was determined using the Crystal Violet colorimetric assay. The percentage of cell growth corresponds to the effect of 2-DG in each indicated transfection condition, as compared to its relative negative control. All values are expressed as means ± SEM of three independent experiments each performed in triplicate. Statistical analysis: * $p<0.05$ siUCP2 versus siCTRL; # o.e. UCP2 versus mock.

**Figure 3.** UCP2 induces Stathmin and hnRNPA2/B1 expression in PaCa44 cells. (**A**) PaCa44 cells were seeded in 60-mm diameter culture dishes and treated with 150 μM genipin for 16 h. 1D-WB analysis was performed with 50 μg of whole cell extracts, probed with the anti-stathmin antibody and PVDF membrane was stained with amido black for control loading. Whole cell extracts obtained as described above were used for 1D-WB (**B**) and 2D-WB (**C**) analyses of hnRNPA2/B1 isoforms. These analyses were representative of three biological replicates. For quantitative analysis, bands were scanned as digital peaks and the areas of the peaks were reported as fold change, as described in Material and Methods. (**D**) HnRNPA2/B1 mRNA expression analysis through qPCR in PaCa44 cells treated with 150 μM genipin for 16 h, or with siRNA UCP2 or the relative negative control (siCTRL), or with the pCMV expression vector containing the human cDNA of UCP2 to overexpress UCP2 (o.e. UCP2) or with empty vector (mock). All values are expressed as means ± SEM of three independent experiments each performed in triplicate. Statistical analysis: * $p<0.05$, ** $p<0.01$ and *** $p<0.001$ genipin versus Ctrl, or siRNA UCP2 versus siCTRL, or o.e. UCP2 versus mock.

**Figure 4.** UCP2 induces the expression of GLUT1 and PKM2 and the secretion of L-lactic acid in PaCa44 cells. (**A**) GLUT1 and PKM2 mRNA expression analysis through qPCR in PaCa44 cells treated with 150 μM genipin for 16 h, or with siRNA UCP2 or the relative negative control (siCTRL), or with the pCMV expression vector containing the human cDNA of UCP2 to overexpress UCP2 (o.e. UCP2) or with empty vector (mock). All values are expressed as means ± SEM of three independent experiments each performed in triplicate. (**B**) Cells were seeded in 60-mm diameter culture dishes and treated with 150 μM genipin for 16 h or (**C**) transfected with siRNA-UCP2 (siUCP2) or its non-targeting siRNA (siCTRL) as negative control. Western blotting was performed with 50 μg of proteins from whole cell extracts probed with the indicated antibodies.

This analysis was representative of three biological replicates. For quantitative analysis, bands were scanned as digital peaks and the areas of the peaks were reported as fold change, as described in Material and Methods. The value of GAPDH was used as a normalizing factor. Statistical analysis: * $p<0.05$ genipin versus CTRL; # $p<0.05$ siUCP2 versus siCTRL. (**D**) PaCa44 cells were set up and processed for IF analysis as detailed in the Material and Methods. GLUT1 protein was revealed by reaction with the specific primary antibody and the secondary antibody conjugated with Alexa Fluor 488. These images are representative of three separate experiments for PaCa44 cells untreated (control) or treated with 150 μM genipin for 16 h. 2D pictures were taken by means of a Leica TCS-SP5 LCM. Nuclei in blue (DAPI) and anti-GLUT1 in green. In the insert box the differential GLUT1 expression levels is highlighted. Scale bar, 20 μm. (**E**) PaCa44 cells were transfected with the plasmid over-expressing UCP2 for 48 h. L-lactic acid level in the culture medium has been analysed by measuring the absorbance at 340nm and the L-lactic acid concentration has been calculated, as detailed in Materials and Methods. Here we report the fold change of the L-lactic acid concentration secreted in the culture medium of cells overexpressing UCP2 versus cells transfected with a mock vector. Statistical analysis: * $p<0.05$ and ** $p<0.01$ genipin versus Ctrl, siUCP2 versus siCTRL, o.e. UCP2 versus mock.

**Figure 5.** UCP2 induces hnRNPA2/B1 and PKM2 through its antioxidant function. PaCa44 cells were seeded in 60-mm diameter culture dishes and treated with 150 μM genipin and/or 20 mM NAC for 16 h. Western blotting was performed with 50 μg of proteins from whole cell extracts probed with the indicated antibodies. This analysis was representative of three biological replicates. For quantitative analysis, bands were scanned as digital peaks and the areas of the peaks were reported as fold change, as described in Material and Methods. The value of amido black staining was used as a normalizing factor. A dashed line delineates cut parts from the same western blot membrane. Statistical analysis: * $p<0.05$, ** $p<0.01$ and *** $p<0.001$ genipin, or NAC or genipin+NAC versus CTRL; or genipin+NAC versus genipin.

**Figure 6.** UCP2 inhibits mitochondrial OXPHOS and oxygen consumption in Panc1 cells. (**A**) Cells were seeded in 6-well plates and transfected with siUCP2 for 4 h at 37 ºC and 5% CO2. Cells were further grown for 48 h and harvested for Western Blot analysis, which has been performed on V-ATP5A-54 kDa (Complex V, subunit alpha), III-UQCRC2-48 kDa (Complex III, subunit Core 2), II-SDHB-29 kDa (Complex II, subunit 30 kDa), IV-COX II-22 kDa (Complex IV, subunit II), and I-NDUFB8-18 kDa (Complex I, subunit NDUFB8). For quantitative analysis, bands were scanned as digital peaks and the areas of the peaks were reported as fold change, as described in Material and Methods. (**B**) COX activity (complex IV) and (C) ATPase activity (complex V) were measured by spectrophotometric methods. (**D**) DNA was extracted from Panc1 cells and a qPCR was performed for a nuclear gene (18S) and a mitochondrial gene (NADH dehydrogenase subunit 4). Values are expressed as the ratio mitochondrial/nuclear gene. (**E**) Basal respiration was measured for 7 min. Maximal respiration was calculated as the difference between the rate after FCCP (8 μM) addition and the rate after antimycin (1 μM) addition. ATP production was calculated as the difference between basal respiration rate and rate after oligomycin addition. Finally, difference between rate after oligomycin addition and rate after antimycin addition was attributed to proton leak. All values are expressed as means ± SEM of three independent experiments each performed in duplicate. Statistical analysis: * $p<0.05$ siUCP2 versus CTRL.

**Figure 7.** Schematic representation of the main metabolic mechanisms regulated by UCP2 identified in this study. Dashed line: multistep reaction. Full line: direct reaction. Italic: enzyme. Green arrow/box: activated pathway/enzyme by UCP2. Red arrow/box: inhibited pathway/enzyme by UCP2. (*): experimentally demonstrated in the present study. Acronyms: Glyceralehyde-3 phosphate: G3P; Glyceralehyde-3 phosphate dehydrogenase: GAPDH; 1,3-biphosphoglycerate: 1,3bisPG; phosphoenolpyruvate: PEP; pyruvate kinase isoform M2: PKM2; pyruvate: PYR; lactate

dehydrogenase: LDH; mtOXPHOS: mitochondrial oxidative phosphorylation; ROS: reactive oxygen species.

**Legends to Supplementary Figures**

**Supplementary Figure 1.** UCP2 mRNA expression levels after UCP2 silencing or overexpression. PaCa44 cells were transfected with (**A**) siRNA UCP2 or the relative negative control (siCTRL), or (**B**) with the pCMV expression vector containing the human cDNA of UCP2 (o.e. UCP2) or with empty vector (mock). All values are expressed as means ± SEM of three independent experiments each performed in triplicate. Statistical analysis: * $p<0.05$ siUCP2 versus siCTRL, or o.e. UCP2 versus mock.

**Supplementary Figure 2.** Effect of 2-DG on PaCa44 cells presenting UCP2 overexpression or knock-down. Panc1 cells were seeded in 96-well plates and transfected for 48 h with pCMV expression vector containing the human cDNA of UCP2 (o.e.UCP2) or with siUCP2. Cell growth was determined by Crystal Violet colorimetric assay. The rate of cell growth inhibition corresponds to the effect of 2.5 mM 2-DG for 48 h as compared to untreated cells, in each indicated transfection condition. Three independent experiments each performed in triplicate were performed for each assay condition. Statistical analysis: * $p<0.05$ o.e.UCP2 or siRNA UCP2 versus Ctrl.

**Supplementary Figure 3.** Representative two-dimensional gel electrophoresis images of PaCa44 cells (**A**) untreated or (**B**) treated with 150 μM genipin for 16 h.

**Supplementary Figure 4.** PANTHER functional classification of the 19 differentially expressed proteins after treatment with the UCP2 inhibitor genipin in pancreas cancer PaCa44 cells. Pie charts show the classification according to (**A**) cellular component, (**B**) biological process and (**C**) molecular function.

**Supplementary Figure 5.** Oxygen consumption rate for control and siUCP2-transfected Panc1 cells. Basal rate was measured and then components modulating mitochondrial function were added sequentially: oligomycin 1 µM, FCCP 8 µM and antimycin 1 µM. Statistical analysis: * $p<0.05$ siUCP2 versus Ctrl.

## References


1 Mailloux, R. J. and Harper, M. E. (2012) Mitochondrial proticity and ROS signaling: lessons from the uncoupling proteins. Trends in endocrinology and metabolism: TEM. **23**, 451-458

2 Pazos, P., Lima, L., Tovar, S., Gonzalez-Touceda, D., Dieguez, C. and Garcia, M. C. (2015) Divergent responses to thermogenic stimuli in BAT and subcutaneous adipose tissue from interleukin 18 and interleukin 18 receptor 1-deficient mice. Scientific reports. **5**, 17977

3 Echtay, K. S. (2007) Mitochondrial uncoupling proteins--what is their physiological role? Free radical biology & medicine. **43**, 1351-1371

4 Toda, C. and Diano, S. (2014) Mitochondrial UCP2 in the central regulation of metabolism. Best practice & research. Clinical endocrinology & metabolism. **28**, 757-764

5 Donadelli, M., Dando, I., Fiorini, C. and Palmieri, M. (2014) UCP2, a mitochondrial protein regulated at multiple levels. Cellular and molecular life sciences : CMLS. **71**, 1171-1190

6 Donadelli, M., Dando, I., Dalla Pozza, E. and Palmieri, M. (2015) Mitochondrial uncoupling protein 2 and pancreatic cancer: a new potential target therapy. World journal of gastroenterology : WJG. **21**, 3232-3238

7 Lopez-Bernardo, E., Anedda, A., Sanchez-Perez, P., Acosta-Iborra, B. and Cadenas, S. (2015) 4-Hydroxynonenal induces Nrf2-mediated UCP3 upregulation in mouse cardiomyocytes. Free radical biology & medicine. **88**, 427-438

8 Ramsden, D. B., Ho, P. W., Ho, J. W., Liu, H. F., So, D. H., Tse, H. M., Chan, K. H. and Ho, S. L. (2012) Human neuronal uncoupling proteins 4 and 5 (UCP4 and UCP5): structural properties, regulation, and physiological role in protection against oxidative stress and mitochondrial dysfunction. Brain and behavior. **2**, 468-478

9 Derdak, Z., Fulop, P., Sabo, E., Tavares, R., Berthiaume, E. P., Resnick, M. B., Paragh, G., Wands, J. R. and Baffy, G. (2006) Enhanced colon tumor induction in uncoupling protein-2 deficient mice is associated with NF-kappaB activation and oxidative stress. Carcinogenesis. **27**, 956-961

10 Dalla Pozza, E., Fiorini, C., Dando, I., Menegazzi, M., Sgarbossa, A., Costanzo, C., Palmieri, M. and Donadelli, M. (2012) Role of mitochondrial uncoupling protein 2 in cancer cell resistance to gemcitabine. Biochimica et biophysica acta. **1823**, 1856-1863

11 Pons, D. G., Nadal-Serrano, M., Torrens-Mas, M., Valle, A., Oliver, J. and Roca, P. (2015) UCP2 inhibition sensitizes breast cancer cells to therapeutic agents by increasing oxidative stress. Free radical biology & medicine. **86**, 67-77

12 Pfefferle, A., Mailloux, R. J., Adjeitey, C. N. and Harper, M. E. (2013) Glutathionylation of UCP2 sensitizes drug resistant leukemia cells to chemotherapeutics. Biochimica et biophysica acta. **1833**, 80-89

13 Derdak, Z., Mark, N. M., Beldi, G., Robson, S. C., Wands, J. R. and Baffy, G. (2008) The mitochondrial uncoupling protein-2 promotes chemoresistance in cancer cells. Cancer research. **68**, 2813-2819

14 Brand, M. D. and Esteves, T. C. (2005) Physiological functions of the mitochondrial uncoupling proteins UCP2 and UCP3. Cell Metab. **2**, 85-93

15 Dando, I., Fiorini, C., Pozza, E. D., Padroni, C., Costanzo, C., Palmieri, M. and Donadelli, M. (2013) UCP2 inhibition triggers ROS-dependent nuclear translocation of GAPDH and autophagic cell death in pancreatic adenocarcinoma cells. Biochimica et biophysica acta. **1833**, 672-679

16 Vyas, S., Zaganjor, E. and Haigis, M. C. (2016) Mitochondria and Cancer. Cell. **166**, 555-566

17 Brandi, J., Dando, I., Palmieri, M., Donadelli, M. and Cecconi, D. (2013) Comparative proteomic and phosphoproteomic profiling of pancreatic adenocarcinoma cells treated with CB1 or CB2 agonists. Electrophoresis. **34**, 1359-1368

18 Dalla Pozza, E., Donadelli, M., Costanzo, C., Zaniboni, T., Dando, I., Franchini, M., Arpicco, S., Scarpa, A. and Palmieri, M. (2011) Gemcitabine response in pancreatic adenocarcinoma cells is synergistically enhanced by dithiocarbamate derivatives. Free radical biology & medicine. **50**, 926-933

19 Kalyanaraman, B., Darley-Usmar, V., Davies, K. J., Dennery, P. A., Forman, H. J., Grisham, M. B., Mann, G. E., Moore, K., Roberts, L. J., 2nd and Ischiropoulos, H. (2012) Measuring reactive oxygen and nitrogen species with fluorescent probes: challenges and limitations. Free radical biology & medicine. **52**, 1-6

20 Robinson, K. M., Janes, M. S. and Beckman, J. S. (2008) The selective detection of mitochondrial superoxide by live cell imaging. Nat Protoc. **3**, 941-947
21 Ayyasamy, V., Owens, K. M., Desouki, M. M., Liang, P., Bakin, A., Thangaraj, K., Buchsbaum, D. J., LoBuglio, A. F. and Singh, K. K. (2011) Cellular model of Warburg effect identifies tumor promoting function of UCP2 in breast cancer and its suppression by genipin. PLoS One. **6**, e24792
22 Zhang, J., Khvorostov, I., Hong, J. S., Oktay, Y., Vergnes, L., Nuebel, E., Wahjudi, P. N., Setoguchi, K., Wang, G., Do, A., Jung, H. J., McCaffery, J. M., Kurland, I. J., Reue, K., Lee, W. N., Koehler, C. M. and Teitell, M. A. (2011) UCP2 regulates energy metabolism and differentiation potential of human pluripotent stem cells. The EMBO journal. **30**, 4860-4873
23 Nie, W., Xu, M. D., Gan, L., Huang, H., Xiu, Q. and Li, B. (2015) Overexpression of stathmin 1 is a poor prognostic biomarker in non-small cell lung cancer. Laboratory investigation; a journal of technical methods and pathology. **95**, 56-64
24 Feng, W., Xiaoyan, X., Xuan, Y., Xiangke, L., Zichang, Y., Ran, Z., Liuxing, W. and Qingxia, F. (2015) Silencing stathmin-modulating efficiency of chemotherapy for esophageal squamous cell cancer with paclitaxel. Cancer gene therapy. **22**, 115-121
25 Jiang, L., Chen, Y., Chan, C. Y., Wang, X., Lin, L., He, M. L., Lin, M. C., Yew, D. T., Sung, J. J., Li, J. C. and Kung, H. F. (2009) Down-regulation of stathmin is required for TGF-beta inducible early gene 1 induced growth inhibition of pancreatic cancer cells. Cancer letters. **274**, 101-108
26 David, C. J., Chen, M., Assanah, M., Canoll, P. and Manley, J. L. (2010) HnRNP proteins controlled by c-Myc deregulate pyruvate kinase mRNA splicing in cancer. Nature. **463**, 364-368
27 Griffin, M. E., Hamilton, B. J., Roy, K. M., Du, M., Willson, A. M., Keenan, B. J., Wang, X. W. and Nichols, R. C. (2004) Post-transcriptional regulation of glucose transporter-1 by an AU-rich element in the 3'UTR and by hnRNP A2. Biochemical and biophysical research communications. **318**, 977-982
28 Li, Q., Liu, X., Yin, Y., Zheng, J. T., Jiang, C. F., Wang, J., Shen, H., Li, C. Y., Wang, M., Liu, L. Z. and Jiang, B. H. (2014) Insulin regulates glucose consumption and lactate production through reactive oxygen species and pyruvate kinase M2. Oxidative medicine and cellular longevity. **2014**, 504953
29 Zhu, J., Bi, Z., Yang, T., Wang, W., Li, Z., Huang, W., Wang, L., Zhang, S., Zhou, Y., Fan, N., Bai, Y., Song, W., Wang, C., Wang, H. and Bi, Y. (2014) Regulation of PKM2 and Nrf2-ARE pathway during benzoquinone induced oxidative stress in yolk sac hematopoietic stem cells. PLoS One. **9**, e113733
30 Dando, I., Dalla Pozza, E., Biondani, G., Cordani, M., Palmieri, M. and Donadelli, M. (2015) The metabolic landscape of cancer stem cells. IUBMB life. **67**, 687-693
31 Stine, Z. E., Walton, Z. E., Altman, B. J., Hsieh, A. L. and Dang, C. V. (2015) MYC, Metabolism, and Cancer. Cancer discovery. **5**, 1024-1039
32 Xu, Y., Miriyala, S., Fang, F., Bakthavatchalu, V., Noel, T., Schell, D. M., Wang, C., St Clair, W. H. and St Clair, D. K. (2015) Manganese superoxide dismutase deficiency triggers mitochondrial uncoupling and the Warburg effect. Oncogene. **34**, 4229-4237
33 Cho, Y. S., Lee, J. H., Jung, K. H., Park, J. W., Moon, S. H., Choe, Y. S. and Lee, K. H. (2016) Molecular mechanism of (18)F-FDG uptake reduction induced by genipin in T47D cancer cell and role of uncoupling protein-2 in cancer cell glucose metabolism. Nuclear medicine and biology. **43**, 587-592
34 Mailloux, R. J. and Harper, M. E. (2011) Uncoupling proteins and the control of mitochondrial reactive oxygen species production. Free radical biology & medicine. **51**, 1106-1115
35 Vozza, A., Parisi, G., De Leonardis, F., Lasorsa, F. M., Castegna, A., Amorese, D., Marmo, R., Calcagnile, V. M., Palmieri, L., Ricquier, D., Paradies, E., Scarcia, P., Palmieri, F., Bouillaud, F. and Fiermonte, G. (2014) UCP2 transports C4 metabolites out of mitochondria, regulating glucose and glutamine oxidation. Proc Natl Acad Sci U S A. **111**, 960-965
36 Samudio, I., Fiegl, M., McQueen, T., Clise-Dwyer, K. and Andreeff, M. (2008) The warburg effect in leukemia-stroma cocultures is mediated by mitochondrial uncoupling associated with uncoupling protein 2 activation. Cancer research. **68**, 5198-5205
37 Mikawa, T., ME, L. L., Takaori-Kondo, A., Inagaki, N., Yokode, M. and Kondoh, H. (2015) Dysregulated glycolysis as an oncogenic event. Cellular and molecular life sciences : CMLS. **72**, 1881-1892
38 Lee, S. B., Kim, C. K., Lee, K. H. and Ahn, J. Y. (2012) S-nitrosylation of B23/nucleophosmin by GAPDH protects cells from the SIAH1-GAPDH death cascade. The Journal of cell biology. **199**, 65-76

39 Cecconi, D. and Zamo, A. (2011) Proteomics of human cancer tissues and cells. Trac-Trend Anal Chem. **30**, 346-359

40 Hart, P. C., Mao, M., de Abreu, A. L., Ansenberger-Fricano, K., Ekoue, D. N., Ganini, D., Kajdacsy-Balla, A., Diamond, A. M., Minshall, R. D., Consolaro, M. E., Santos, J. H. and Bonini, M. G. (2015) MnSOD upregulation sustains the Warburg effect via mitochondrial ROS and AMPK-dependent signalling in cancer. Nature communications. **6**, 6053

41 Maldonado, E. N., Sheldon, K. L., DeHart, D. N., Patnaik, J., Manevich, Y., Townsend, D. M., Bezrukov, S. M., Rostovtseva, T. K. and Lemasters, J. J. (2013) Voltage-dependent anion channels modulate mitochondrial metabolism in cancer cells: regulation by free tubulin and erastin. J Biol Chem. **288**, 11920-11929

# The antioxidant uncoupling protein 2 stimulates hnRNPA2/B1, GLUT1 and PKM2 expression and sensitizes pancreas cancer cells to glycolysis inhibition

Jessica Brandi[1*], Daniela Cecconi[1*], Marco Cordani[2*], Margalida Torrens-Mas[3], Raffaella Pacchiana[2], Elisa Dalla Pozza[2], Giovanna Butera[2], Marcello Manfredi[4,5], Emilio Marengo[4], Jordi Oliver[3], Pilar Roca[3], Ilaria Dando[2#], Massimo Donadelli[2#].

[1]*Department of Biotechnology, Proteomics and Mass Spectrometry Laboratory, University of Verona, Verona, Italy;*

[2]*Department of Neuroscience, Biomedicine and Movement, Biochemistry Section, University of Verona, Verona, Italy;*

[3]*Multidisciplinar Group of Translational Oncology, University Research Institute on Health Sciences (IUNICS), University of the Balearic Islands, E07122, Palma, Spain; Palma Institute for Health Research (IdISPa), E07010 Palma, Spain; Physiopathology of Obesity and Nutrition, CIBERobn (CB06/03), Carlos III Health Research Institute (ISCIII), Madrid, Spain;*

[4]*Department of Sciences and Technological Innovation, University of Eastern Piedmont, Alessandria, Italy;*

[5]*ISALIT, Novara, Italy.*

* *These authors equally contributed and share the first authorship*.

**[#]Corresponding authors:**

Massimo Donadelli, PhD. Department of Neuroscience, Biomedicine and Movement. Biochemistry Section, University of Verona, Verona, Italy. Strada Le Grazie 8, 37134 Verona, Italy.

phone: +39 045 8027281; fax: +39 045 8027170; e-mail: massimo.donadelli@univr.it

Ilaria Dando, PhD. Department of Neuroscience, Biomedicine and Movement. Biochemistry Section, University of Verona, Verona, Italy. Strada Le Grazie 8, 37134 Verona, Italy.

phone: +39 045 8027174; fax: +39 045 8027170; e-mail: ilaria.dando@univr.it

*Running title:* UCP2 sensitizes cancer cells to 2-DG

*Keywords:* cancer, metabolism, uncoupling proteins, UCP2, Warburg effect, proteomics.

**Abstract**

Several evidence indicate that metabolic alterations play a pivotal role in cancer development. Here, we report that the mitochondrial uncoupling protein 2 (UCP2) sustains the metabolic shift from mitochondrial oxidative phosphorylation (mtOXPHOS) to glycolysis in pancreas cancer cells. Indeed, we show that UCP2 sensitizes pancreas cancer cells to the treatment with the glycolytic inhibitor 2-deoxy-D-glucose. Through a bidimensional electrophoresis analysis, we identify 19 protein species differentially expressed after treatment with the UCP2 inhibitor genipin and, by bioinformatic analyses, we show that these proteins are mainly involved in metabolic processes. In particular, we demonstrate that the antioxidant UCP2 induces the expression of hnRNPA2/B1, which is involved in the regulation of both GLUT1 and PKM2 mRNAs, and of lactate dehydrogenase (LDH) increasing the secretion of L-lactic acid. We further demonstrate that the radical scavenger *N*-acetyl-$_{L}$-cysteine reverts hnRNPA2/B1 and PKM2 inhibition by genipin indicating a role for reactive oxygen species in the metabolic reprogramming of cancer cells mediated by UCP2. We also observe an UCP2-dependent decrease in mtOXPHOS complex I (NADH dehydrogenase), complex IV (cytochrome c oxidase), complex V (ATPase) and in mitochondrial oxygen consumption, suggesting a role for UCP2 in the counteraction of pancreatic cancer cellular respiration. All these results reveal novel mechanisms through which UCP2 promotes cancer cell proliferation with the concomitant metabolic shift from mtOXPHOS to the glycolytic pathway.

## 1. Introduction

Uncoupling proteins (UCPs) are mitochondrial anion transporter proteins localized into the mitochondrial inner membrane [1]. Currently, five UCP family members have been identified in mammals. Among them, UCP1 is highly expressed in brown adipose tissue playing a key role in adaptive non-shivering thermogenesis [2]. UCP2 (59% of amino acid sequence in common with UCP1) is widely distributed throughout the organism, suggesting different and wide functions for this mitochondrial uncoupling protein [3]. As a result of its ubiquitous distribution, UCP2 has been indicated to participate in several metabolic processes [4] and its misregulation is linked with the development of several diseases, including cancer [5, 6]. UCP3 is most abundantly expressed in skeletal muscle and, to a lesser extent, in brown adipose tissue and heart, and might play important roles in attenuation of reactive oxygen species (ROS) production and fatty acid metabolism [7]. Both UCP4 and UCP5 uncoupling family members are likely involved in the protection of neurons from an excessive production of ROS. They are primarily expressed in the central nervous system with marked dissimilarities in the expression level in different areas of the brain [8].

Among the various physio-pathological functions of UCP family members, the role of UCP2 in cancer has been recently recognized and attracted more attention. Many studies have well established the key role that UCP2 has in both tumorigenesis and chemoresistance. The generally accepted suggestion envisages that, during the first stages of tumorigenesis, UCP2 is down-regulated likely to allow ROS increase and genomic instability [6, 9], while it is triggered or over-expressed in the following stages of cancer development, finally determining resistance of cancer cells to therapies and tumor aggressiveness mainly through anti-apoptotic mechanisms induced by the attenuation of mitochondrial ROS production. This last item has been widely demonstrated in several cancer types, including pancreatic adenocarcinoma [10], breast cancer [11], leukemia cells [12], and drug-resistant colon cancer cells [13]. The antioxidant effect of UCP2 is mainly due by the transport of protons from the intermembrane space to the mitochondrial matrix bypassing ATP synthase. This event results in a decrease of several consequential events, as mitochondrial inner

membrane potential, electron leakage from respiratory electron transport chain and superoxide ion generation into mitochondrial matrix. Therefore, mild uncoupling of mitochondrial oxidative phosphorylation (mtOXPHOS) may represent the first line of defense against oxidative stress in cancer cells by decreasing mitochondrial respiration [14, 15]. Overall, since mitochondria are crucial organelles that can allow cancer cells to adapt to environmental alterations they are considered important mediators of tumor progression [16].

In the present study, we further investigated the involvement of mitochondrial UCP2 in biological and, especially, metabolic processes associated with pancreatic cancer cell proliferation. Overall, by using a proteomic approach we demonstrated that UCP2 regulates a number of crucial metabolic enzymes/proteins. In particular, we proved that UCP2 triggers the expression of: i) the heterogeneous nuclear ribonucleoprotein A2/B1 (hnRNPA2/B1); ii) the glucose transporter GLUT1; iii) the pyruvate kinase isoform M2 (PKM2); and iv) the lactate dehydrogenase (LDH) resulting in enhanced secretion of L-lactic acid. Overall these findings suggest that UCP2 promotes the glycolytic phenotype, thus determining an enhancement of cancer cell sensitivity to the glycolysis inhibitor 2-deoxy-D-glucose (2-DG). Furthermore, we observed that UCP2 reduces mitochondrial oxygen consumption and mtOXPHOS functionality without altering the overall amount of mtDNA. Finally, our results sustain the role of UCP2 as a crucial mediator in cancer cellular bioenergetic shift from mtOXPHOS to the glycolytic pathway.

## 2. Material and Methods

### *2.1 Chemicals*

Genipin (methyl-2-hydroxy-9-hydroxymethyl-3-oxabicyclonona-4,8-diene-5-carboxylate) and 2-deoxy-D-glucose (2-DG) were obtained from Sigma (Milan, Italy), solubilized in DMSO and bi-distillated sterile water, respectively, and stored at -80 °C until use. *N*-acetyl-$_L$-cysteine (NAC) was obtained from Sigma and solubilized in bi-distillated sterile water.

### *2.2 Cell culture*

Human pancreatic adenocarcinoma cell lines PaCa44 and Panc1 were grown in RPMI medium (Life Technologies, Milan, Italy), supplemented with 10% FBS, and 50 μg/ml gentamicin sulfate (BioWhittaker, Lonza, Bergamo, Italy). Cell lines were incubated at 37 °C with 5% $CO_2$.

### *2.3 Cell proliferation assay*

Cells were seeded in 96-well plates ($5\times10^3$ cells/well) and the day after were incubated with various compounds at the indicated conditions or transfected with the indicated constructs (see figure legends). At the end of the treatments, cell growth was measured by Crystal Violet assay (Sigma, Milan, Italy) according to the manufacturer's protocol, and absorbance was measured by spectrophotometric analysis ($A_{595}$nm).

### *2.4 Transient transfection assays*

Exponentially growing cells were seeded at a density of $5\times10^3$ cells/well in 96-well plates for proliferation assays and at $2.5x10^5$ cells/plate in 60 mm cell culture plates for protein extraction. The ectopic over-expression of UCP2 in cancer cells was carried out transfecting for 48 h the pCMV expression vector containing the human cDNA of UCP2 (OriGene Technologies, Rockville, MD) using Lipofectamine 3000 transfection reagent according to the manufacturer's instructions

(Thermo Fisher, Milan, Italy). Cells transfected with the pCMV empty vector were used as negative control (mock). Knock-down of UCP2 expression was obtained by transfecting cells with a specific small interfering (si) (5'-GCUAAAGUCCGGUUACAGATT-3') RNA targeting UCP2 mRNA and a non-targeting siRNA (5'-CAGUCGCGUUUGCGACUGG-3') used as negative control purchased by Ambion (Monza MB, Italy). Cells were transfected with siRNAs at a final concentration of 50 nM using Lipofectamine 3000 transfection reagent for 48 h (Thermo Fisher, Milan, Italy).

*2.5 RNA extraction and qPCR*

Total RNA was extracted from $10^6$ cells using TRIzol Reagent (Life Technologies, Milan, Italy), and 1 µg of RNA was reverse transcribed using first-strand cDNA synthesis. Real-time quantification was performed in triplicate samples by SYBR Green detection chemistry with Power SYBR Green PCR Master Mix (Applied Biosystems) on a 7000 Sequence Detection System. The primers used were: Hs_UCP2_1_SG QuantiTect Primer Assay (Qiagen, Milan, Italy) for the UCP2 gene; hnRNPA2/B1 F: 5'-AGC TTT GAA ACC ACA GAA GAA-3', hnRNPA2/B1 R: 5'-TTG ATC TTT TGC TTG CAG GA-3'; GLUT1 F: 5'-CAT CAT CTT CAT CCC GGC-3', GLUT1 R: 5'-CTC CTC GTT GCG GTT GAT-3'; PKM2 F: 5'-CAG AGG CTG CCA TCT ACC AC-3', PKM2 R: 5'-CCA GAC TTG GTG AGG ACG AT-3'; and Hs_RRN18S_1_SG QuantiTect Primer Assay for 18S rRNA. The thermal cycle reaction was performed as follows: 95 °C for 10 minutes followed by 40 cycles at 95 °C for 15 seconds and 60°C for 1 minute. Three independent experiments were performed for each assay condition.

*2.6 2DE proteomics analysis*

2DE protein analysis from $1.5x10^6$ PaCa44 cells, untreated and treated with 150 µM genipin for 16 h, was performed as previously described [17]. Briefly, 500 µg of protein were subjected to IEF with 17 cm immobilized nonlinear pH 3–10 gradient IPG strips using a Protean IEF Cell (Bio-

Rad). After IEF, IPG strips were equilibrated and then the proteins were separated using 8–18% SDS-PAGE gels. Ruthenium chelate (RuBPs) fluorescent staining was used to visualize protein spots on 2DE gel. The protein pattern differential analysis of 10 stained gels (5 technical replicates x 2 samples, i.e. control and genipin treated cells) were performed by PDQuest software v7.3 (Bio-Rad).

*2.7 Protein identification by nano-HPLC-Chip ion trap MS/MS*

Protein identification was performed after in-gel trypsin digestion, as previously described [17]. Briefly, peptides from each sample were separated by RP nano-HPLC-Chip technology (Agilent Technologies, Palo Alto, CA, USA) online-coupled with a 3D ion trap mass spectrometer (model Esquire 6000, Bruker Daltonics, Bremen, Germany). Database searches were conducted using the MS/MS ion search of Mascot against human entries of the non-redundant NCBI database.

*2.8 Protein annotation and enriched pathways analysis*

Functional annotation of identified proteins was performed according to Gene Ontology (GO) using the PANTHER classification system v 9.0 (http://www.pantherdb.org/) according to biological processes, molecular functions and cellular components. Enrichment pathways analysis was done using STRING 9.1 database (http://string-db.org). Gene Ontology terms and enriched pathways were considered significant for adjusted p-values lower than 0.05.

*2.9 Immunoblot analysis*

Cells were harvested, washed in PBS, and re-suspended in lysis buffer in the presence of phosphatase and protease inhibitors (50 mM Tris–HCl pH 8, 150 mM NaCl, 1% Igepal CA-630, 0.5% Na-Doc, 0.1% SDS, 1 mM $Na_3VO_4$, 1 mM NaF, 2.5 mM EDTA, 1 mM PMSF, and 1× protease inhibitor cocktail). After incubation on ice for 30 min, the lysates were centrifuged at 14,000 × g for 10 min at 4 °C and the supernatant fractions were used for Western blot analysis.

Protein concentration was measured by Bradford reagent (Pierce, Milan, Italy) using bovine serum albumin as a standard. Protein extracts (50 μg/lane) were resolved on a 12% SDS-polyacrylamide gel and electro-blotted onto PVDF membranes (Millipore, Milan, Italy). Membranes were blocked in 5% low-fat milk in TBST (50 mM Tris pH 7.5, 0.9% NaCl, 0.1% Tween 20) for 1 h at room temperature and probed overnight at 4 °C with goat polyclonal anti-UCP2 (1:1000) (Abnova), rabbit anti-GLUT1 (1:1,000) (Abcam, #ab652), rabbit polyclonal anti-phospho-(Tyr105)PKM2 (1:1,000) (Cell Signaling #3827), mouse polyclonal anti-PKM2 (1:1,000) (Sigma # WH0005315M1), mouse anti-hnRNPA2/B1 (1:400) (Santa Cruz sc-374053), rabbit anti-stathmin 1 (1:5,000) (Sigma Aldrich O-01238), antisera against mtOXPHOS complexes (MitoSciences, OR, USA), or rabbit monoclonal glyceraldehyde 3-phosphate dehydrogenase (GAPDH) (1:1,000) (Cell Signaling, #5174S) antibodies. Horseradish peroxidase conjugated anti-mouse, anti-goat or anti-rabbit IgGs (1:8,000 in blocking solution) (Upstate Biotechnology, Milan, Italy) were used as secondary antibodies. Immunodetection was carried out using chemiluminescent substrates and recorded using a HyperfilmECL (Amersham Pharmacia Biotech). ECL results were scanned and the amount of each protein band quantitated using NIH Image J software (http://rsb.info.nih.gov/nih-image/).

*2.10 L-lactic acid quantification in culture medium*

After the transfection period, culture medium has been taken and diluted 30-fold in $H_2O$. For each sample 25 μl has been analyzed in a final reaction volume of 500 μl (Megazyme, #K-LATE 07/14). Absorbance at 340 nm has been read after 10 minutes the activation of the reaction and L-lactic acid concentration (g/L) has been calculated according to the manufacturer's instructions.

*2.11 Measurement of mitochondrial superoxide production*

The non-fluorescent MitoSox Red probe (Molecular Probes, Thermo Fisher, Milan, Italy) was used to evaluate mitochondrial $O_2$•− production as described in [18]. Briefly, cells were seeded

in 96-well plates ($5\times10^3$ cells/well) and, the day after, treated with 150 µM genipin for 16 h. At the end of treatment, cells were incubated in culture medium with 0.5 µM MitoSox probe at 37 °C for 15 min. Cells were washed with Hanks buffer (20 mM Hepes pH 7.2, 10 mM glucose, 118 mM NaCl, 4.6 mM KCl, and 1 mM $CaCl_2$) and fluorescence was measured by using a multimode plate reader (Ex 430 nm and Em 590 nm) (GENios Pro, Tecan, Milan, Italy). The probe is live-cell permeant and is rapidly and selectively targeted to the mitochondria where it becomes fluorescent after oxidation by $O_2$•−. The usage of 430±35 nm of excitation wavelengths allowed us to selectively detect mitochondrial $O_2$•− strongly reducing the recognition of other oxidants (e.g., •OH, ONOO•−) [19, 20]. The values were normalized on cell proliferation by Crystal Violet assay.

*2.12 Immunofluorescence (IF) and Laser Confocal Microscopy (LCM)*

PaCa44 cells treated or untreated with genipin were fixed in 4% paraformaldehyde (PFA; 15 min) and, after 4 changes (10 min each) of PBS, were permeabilized in 0.1% Triton X–100 (5 min) in PBS. To saturate unspecific binding sites, the cells were incubated for 45 min at room temperature (RT) with a blocking solution containing 5% BSA and 0.05% Triton X-100 in PBS. Samples were then incubated overnight at 4 °C with anti-GLUT1 (1:500) (from Abcam, Cambridge, UK) primary antibody diluted in blocking solution. After 3 washes with PBS (10 min each), cells were incubated for 1h at RT in the dark with specific secondary antibodies (1µg/mL) conjugated with Alexa Fluor-488 (Molecular Probes, Invitrogen Corporation, Carlsbad, CA). The incubation with secondary antibodies was followed by a 10 min incubation with 1.0 µg/mL of 4′, 6-diamidino-2-phenylindole dihydrochloride (DAPI, Sigma). Coverslips were mounted in anti-bleaching medium (Dako Fluorescent Mounting Medium, Dako, CA, USA). The negative control procedure omitted the primary antibody.

LCM acquisition was performed using a Leica TCS SP5 AOBS microscope (Leica–Microsystems, Wezlar, Germany) equipped with violet (405 nm laser diode), blue (argon, 488 nm), orange (543 nm) and red (633 nm, HeNe laser) excitation laser lines. A 63x / 1.40 NA oil-

immersion objective (HCX PL APO 63x 1.40 OIL UV, Leica-Microsystem) was employed for the analysis. The acquisition conditions were set to prevent fluorescence loss and to cause minimal photo-damage. All images were acquired with the following sequential settings: zoom 2.0; format 2048 x 2048; pixel size 0.120 x 0.120 µm and pinhole was set to 1.0 Airy unit.

*2.13 Mitochondrial membrane potential (ΔΨm)*

Mitochondrial membrane potential was measured fluorimetrically by using tetramethylrhodamine methyl ester (TMRM) probe. PaCa44 cells were seeded in 96-well plates ($7x10^3$ cells/well) and treated with 150 µM genipin for 16 h or transfected with siRNA-UCP2 for 48 h. After treatment, cells were exposed to 100 nM TMRM for 15 min and fluorescence measurement was performed in an FLx800 microplate fluorescence reader (Bio-Tek Winooski, VT, USA) set at excitation and emission wavelengths of 552 and 576 nm. Values were normalized per number of viable cells determined by crystal violet assay.

*2.14 Enzymatic activities*

Cells were harvested 48h after transfection by scraping them into 200 µl of STE buffer (250 mM sucrose, 3.59 mM Trizma-Base, 16.4 Tris-HCl pH 7.4, 2 mM EDTA, 40 mM KCl). Then, cells were disrupted by sonication at 40% amplitude for 10 seconds three times (VibraCell 75185) and centrifuged at 600 × g for 10 min at 4 °C to remove cell debris. Protein content (supernatant) was determined with a bicinchoninic acid (BCA) protein assay kit (Pierce, Bonn, Germany) and the enzymatic assays were performed immediately after.

Cytochrome c oxidase (COV, Complex IV, EC 1.9.3.1) activity was measured using a spectrophotometric assay. Briefly, cell lysate was incubated in 0.1 M $NaPO_4H_2$, pH 7.0 in the presence of 2 µg/mL catalase and 5 mM substrate DAB (3,3'-diaminebenzidine-tetrachloride) and then 100 µM of reduced cytochrome c was added to start the reaction. The absorbance increment

was followed for 25 min at 450 nm and 37 °C. The generated slope is directly proportional to the activity of COX.

ATP synthase (ATPase, ATP phosphohydrolase, Complex V, EC 3.6.1.3) activity was measured by following the oxidation of NADH at 340 nm and 37 °C. Briefly, cell lysate was incubated in assay buffer (0.33 M sucrose, 6.3 mM $MgSO_4$, 63.66 mM HEPES, 0.442 mM NADH, pH 8.0) in the presence of 2.5 mM Phospho(enol)pyruvic acid, 0.5 µg/mL Pyruvate Kinase, 0.25 µg/mL l-Lactic dehydrogenase and 0.1 µg/mL antimycin. Then, 5 mM ATP was added to start the reaction. The extinction coefficient used was 6.22 $mM^{-1}cm^{-1}$. The absorbance reduction was followed for 15 min and the maximum slope was taken to analyze activity data. The generated slope is inversely proportional to the activity of ATPase.

*2.15 mtDNA quantification*

DNA was isolated from cultured cells using the innuPREP DNA Mini Kit (Analytik Jena) following the manufacture protocol. The extracted DNA was quantified using a spectrophotometer (BioSpec-nano) to amplify 5 ng of DNA using specific primers for 18S and the NADH dehydrogenase subunit 4 (mitochondrial) with SYBR Green Technology on a LightCycler 480 System II (Roche Diagnostics, Basel, Switzerland). Total reaction volume was 10 µL, containing 7.5 µL Lightcycler® 480 SYBR Green I Master, 0.5 µM of the sense and antisense specific primers and 2.5 µL of the DNA. The thermal cycle reaction was performed as follows: 95 °C for 5 minutes followed by 45 cycles at 95 °C for 10 seconds and 60 °C for 10 seconds, and an extension step at 72 °C for 12 seconds. A negative control without cDNA template was run for each gene. The primers used were forward 5'-GGA CAC GGA CAG GAT TGA CA-3' and reverse 5'-ACC CAC GGA ATC GAG AAA GA-3' for 18S, and forward 5'-CGT GAC TCC TAC CCC TCA CA-3' and reverse 5'-ATC GGG TGA TGA TAG CCA AG- 3' for the NADH dehydrogenase subunit 4 (mtDNA) .The Ct values of the real-time PCR were analysed, referring these results to the total DNA amount, using the GenEx Standard Software (MultiDAnalises, Sweden).

*2.16 Oxygen consumption rate*

After transfection, cells were harvested and 1.25 x $10^6$ cells were incubated in 0.5 mL of DMEM in a water-thermostatically regulated chamber with a computer-controlled Clark-type $O_2$ electrode (Oxygraph; Hansatech, Norfolk, UK). Cells were preincubated for 5 min at 37 °C and basal respiration rate was measured. Next, 1 µM oligomycin was added to the chamber to reveal ATP synthase-dependent oxygen consumption. Then, 8 µM FCCP was added to observe maximal respiration and finally 1 µM antimycin was added to inhibit the electron transport chain and stop mitochondrial oxygen consumption. Each oxygen consumption rate was measured three times during 7 min.

*2.17 Statistical analyses*

ANOVA (post hoc Bonferroni) analysis was performed by GraphPad Prism 5 software. p values < 0.05 and 0.01 were indicated as (*) or (**), respectively. In 2-DE image analysis, Student's t test ($p < 0.05$) was applied on log-transformed protein volumes normalized by intensities of all valid spots using PDQuest (Bio-Rad). Multivariate statistics of 2DE image analysis was performed with Simca-P+ v12.0 (Umetrics, Sweden). In particular for identification of proteins separating control from genipin-treated cells, we used orthogonal partial least squares discriminant analysis (OPLS-DA), applying a variable influence on projection (VIP) >1.5 to identify the protein spots that contributed most to the calculated OPLS-DA model. We only considered protein spots that showed good correlations [p(corr)>0.7] by the multivariate OPLS-DA and that differed from controls with significances better than $p<0.05$ by using the Student's t test.

## 3. Results

### *3.1 The antioxidant mitochondrial uncoupling protein UCP2 sensitizes pancreatic cancer cells to the glycolytic inhibitor 2-DG*

To investigate novel molecular mechanisms and metabolic alterations driven by UCP2 in pancreatic cancer cells we overexpressed or down-regulated UCP2 expression using transient transfection tools described in Material and Methods section. Furthermore, we also used genipin, a pharmacological inhibitor of UCP2 activity, to confirm some crucial results obtained in the present study. We first aimed to confirm the selective effect of genipin on UCP2 inhibition analyzing the outcome of this drug in pancreatic cancer cell growth in UCP2-deficient conditions. **Figure 1A** shows that UCP2 knockdown by a specific siRNA-UCP2 significantly reduced the antiproliferative effect of genipin in PaCa44 cells. In addition, genipin was able to increase mitochondrial superoxide production and mitochondrial membrane potential in pancreatic cancer cells. Indeed, genipin increased both the mitochondrial superoxide level in PaCa44 cells (~20-folds) (**Figure 1B**) and the proton gradient in the inner mitochondrial membrane (71%), as did the siUCP2 (41%) (**Figure 1C**). Altogether these data support the specific effect of genipin on the inhibition of the antioxidant mitochondrial uncoupling protein UCP2 in our experimental system.

Since UCP2 has been previously described to support the glycolytic phenotype [21, 22], we here aimed to analyze whether the sensitivity of pancreatic cancer cells to glycolysis inhibitors might be influenced by UCP2 expression. In order to achieve this purpose we evaluated the response of pancreatic cancer cells to 2-deoxy-D-glucose (2-DG), a stable glucose analogue widely used as a glycolytic flux inhibitor, after knockdown or overexpression of UCP2. The effective modulation of UCP2 expression by transfection tools has been confirmed with qPCR experiments (**Supplementary Figure 1**). Our data show that the transient knockdown of UCP2 significantly decreased the sensitivity of PaCa44 cells to 2-DG if compared to its negative control (**Figure 2A**), while, UCP2 overexpression conferred a strong sensitization to 2-DG incubation, as compared to its

relative mock vector (**Figure 2B**). Similar results were obtained in another pancreatic cancer cell line, Panc1 cells (**Supplementary Figure 2**). Overall, these results demonstrated that the oncogenic properties of UCP2 might be specifically counteracted by targeting glycolysis, thus representing a novel and effective therapeutic strategy for pancreas cancer patients having high UCP2 expression levels.

*3.2 Bidimensional proteomic profiling of pancreatic cancer cells treated with the UCP2 inhibitor genipin*

To unravel novel molecular insights related to the regulation of pancreatic cancer cell growth and metabolism by UCP2 we performed a bidimensional proteomic profiling of PaCa44 cells treated with genipin. **Supplementary Figure 3** shows representative 2D gels from untreated and genipin-treated cells. About 500 polypeptide spots were revealed in the pH 3-10 interval with the high-sensitivity RuBPs stain, and then matched between the different gels. To quantify level changes of individual spots and also to detect interrelationships between them and thereby explore categories of differential protein expression, the normalized spot volumes were subjected to both univariate and multivariate statistics analysis. The criteria used for protein identification choice with a difference greater than 30%, with $p< 0.05$ by Student's *t* test, and/or with p(corr)>0.7 by the multivariate OPLS-DA, yielded 24 apparent protein spots. All these modulated spots were successfully picked up and a total of 19 protein species were identified by nano-HPLC-Chip ion trap MS/MS and detailed in **Table 1**. By bioinformatic analyses, we found that the cellular components mostly over-represented in genipin-treated cells were extracellular exosome (28%), extracellular membrane-bounded organelle (17%), membrane-bounded organelle (17%) and cytosol (17%). In addition, the GO enrichment analysis suggests that the identified proteins are mainly involved in metabolic process (31%), cellular process (18%) and component organization (13%), as well as developmental process (13%). As concerning the molecular function category, we found

among the most prominent significant GO enriched terms the catalytic activity (59%), binding (17%), and structural molecule activity (12%) (**Supplementary Figure 4**).

Among the 19 identified protein species by 2DE analysis reported in Table 1 some are related with the promotion of cancer cell proliferation by UCP2, in accordance with our previous discoveries [10, 15]. Indeed, the expression of one form of stathmin 1 is decreased 1.37 fold in PaCa44 cells treated with genipin in comparison to untreated cells (Table 1). Furthermore, this result has been validated by 1D-WB in PaCa44 cells treated with genipin showing a decreased expression of stathmin 1 in comparison to control cells (**Figure 3A**). Stathmin 1 has been proposed as a potential prognostic marker for patients with non-small cell lung cancer [23] and has been shown to lead resistance to chemotherapeutic agents in human esophageal squamous cancer cells [24], whose overexpression prevented TGFβ-mediated growth inhibition of pancreatic cancer cells [25], suggesting a role for stathmin 1 in the UCP2-mediated chemoresistance of pancreas cancer cells.

Interestingly, the protein hnRNPA2/B1, a known regulator of the alternative splicing of the glycolytic enzyme pyruvate kinase (PK) [26], is strongly repressed (<20 fold) by genipin in PaCa44 cells (Table 1). Thus, we also validated by 1D-WB the protein hnRNPA2/B1, whose expression strongly decreased in PaCa44 cells treated with genipin in comparison to control cells (**Figure 3B**). Furthermore, 2DE-WB analysis of hnRNPA2/B1 revealed six signals in untreated cells at pI from ~7 to ~9 and the most basic protein isoform appears to be present only in untreated cells, while it is absent in cells treated with genipin (**Figure 3C**), in accordance with the proteomic data (Table 1). The qPCR approach further revealed that UCP2 inhibition by genipin or siUCP2 significantly repressed hnRNPA2/B1 mRNA expression, while UCP2 overexpression enhanced its mRNA level, strongly suggesting a transcriptional regulation of hnRNPA2/B1 gene driven by UCP2 (**Figure 3D**).

*3.3 UCP2 stimulates GLUT1 and PKM2 expression in pancreatic cancer cells*

Since hnRNPA2 family members have been found to bind and regulate GLUT1 mRNA expression in cancer cells [27] and the alternative splicing of the pyruvate kinase isoform M2 (PKM2) by including the exon 10 in the mRNA [26], we investigated whether UCP2 might trigger the up-regulation of both GLUT1 and PKM2 expression, in addition to the induction of hnRNPA2/B1. Accordingly, we demonstrated that UCP2 inhibition by genipin or siUCP2 significantly repressed both GLUT1 and PKM2 mRNA expression levels, while UCP2 overexpression enhanced their mRNA levels (**Figure 4A**). These data were further confirmed at the protein level by Western blot assay. Indeed, both GLUT1 and PKM2 protein expression levels were down-modulated after treatment with genipin (**Figure 4B**) or siUCP2 (**Figure 4C**). We further observed a marked reduction of GLUT1 expression in genipin-treated cells as compared to control cells by using confocal microscopy immunofluorescence (**Figure 4D**), thus confirming the involvement of UCP2 in the up-regulation of GLUT1 in pancreatic cancer cells. Finally, the quantification of the L-lactic acid in the cell culture medium showed that UCP2 over-expression significantly increased the secretion of L-lactic acid in comparison to negative control (**Figure 4E**), thus supporting the stimulation of the glycolytic phenotype by UCP2 in pancreatic cancer cells and the enhancement of the UCP2-related sensitivity of these cells to the glycolytic inhibitor 2-DG (Figure 2).

*3.4 The antioxidant function of UCP2 is involved in hnRNPA2/B1 and PKM2 stimulation*

To further investigate the bases of the metabolic modifications driven by UCP2 we analyzed whether the antioxidant function of UCP2 might have a role in the stimulation of hnRNPA2/B1 and PKM2. First, we confirmed that UCP2-inhibition by genipin was able to induce mitochondrial ROS production in these cells (Figure 1B). Furthermore, the addition of the radical scavenger *N*-acetyl-$_{L}$-cysteine (NAC), previously described by our group to be able to revert the antiproliferative effects induced by genipin in these cells [15], strongly rescued both hnRNPA2/B1 and PKM2 expression inhibition by genipin (**Figure 5**). The observed down-modulation of PKM2 expression by both the

pro-oxidant agent genipin and the antioxidant NAC alone might be explained by previous data reporting that the alteration of the overall cellular redox status might modify PKM2 expression [28, 29]. Altogether these results suggest that the glycolytic pathway triggered by UCP2 in pancreatic cancer cells might be mainly assured by its antioxidant function.

*3.5 UCP2 counteracts pancreatic cancer cellular respiration inhibiting mtOXPHOS and oxygen consumption*

To further evaluate the effects of UCP2 on mitochondrial metabolism, we also performed different analyses on OXPHOS mitochondrial complexes and oxygen consumption rate. We observed a general increase in all OXPHOS complexes with siUCP2, which resulted significant for the subunit NDUFB8 of the complex I (NADH dehydrogenase), the subunit COX II of the complex IV (cytochrome c oxidase) and the subunit ATP5A of the complex V (ATPase), as shown in **Figure 6A**. Furthermore, both enzymatic activities of complex IV and complex V significantly increased by 27% and 25%, respectively, when UCP2 was knocked-down (**Figure 6B** and **6C**). On the other hand, we evaluated the mitochondrial DNA (mtDNA) content to check whether there was an increase in the overall amount of mitochondria after UCP2 inhibition. As shown in **Figure 6D**, cells transfected with siUCP2 did not show any changes in mtDNA copy number. As shown in **Figure 6E** and **Supplementary Figure 5** basal oxygen consumption rate (OCR) was significantly higher in UCP2-knockdown cells compared to control ones. The difference between basal rate and rate after oligomycin addition corresponds to the oxygen consumed for ATP production, which is higher in siUCP2 transfected cells. The mitochondrial uncoupler FCCP and antimycin were sequentially added to evaluate maximal cellular respiration. Finally, maximal respiration, calculated as the difference between the rate after FCCP addition and the rate after antimycin addition, was also greater in cells with UCP2 knockdown (Figure 6E).

**4. Discussion**

Nowadays, the study of the metabolic aberrations in cancer disease is very intense and debated since they might represent a therapeutic target to selectively inhibit neoplastic proliferation [30, 31]. In a recent article, Xu *et al.* stated that mitochondrial uncoupling mediated by UCPs leads the shift of cell metabolism from mtOXPHOS to aerobic glycolysis, also named Warburg effect, as a metabolic adaptation of cancer cells bearing antioxidant-deficient mitochondria [32]. Data presented by Xu *et al.* support the previous knowledge about UCP2 involvement in the maintenance of Warburg effect in cancer, as demonstrated by the high production of lactate after overexpression of uncoupling proteins [13]. Recently, Cho *et al.* demonstrated that genipin or siRNA-UCP2 strongly reduced the uptake of $^{18}$F-fluoro-deoxyglucose and consequently the secretion of lactate in breast and colon cancer cells [33].

In addition to the antioxidant property of UCP2 by allowing the flux of protons from the mitochondrial intermembrane space to the mitochondrial matrix [34], the channel formed by this protein can also promote the mitochondrial efflux of pyruvate and of Krebs cycle intermediates towards the cytosol, thus limiting the mitochondrial oxidation of glucose- and glutamine-derived metabolic intermediates [35]. Furthermore, Samudio *et al.* revealed that the exposure of leukemia cells to mesenchymal stromal cells results in increased accumulation of lactate in the culture medium, indicative of the Warburg effect. Most notably, the increased glycolytic phenotype is accompanied by decreased mitochondrial membrane potential in the leukemic cells as a result of mitochondrial uncoupling promoted by UCP2, suggesting that the Warburg effect mediated by uncoupling proteins might also be triggered by cancer-stroma crosstalk [36]. Accordingly, Zhang *et. al*. further demonstrated that during early differentiation human pluripotent stem cell proliferation slows, energy metabolism decreases, and UCP2 expression is repressed, resulting in decreased glycolysis and preserved or increased mitochondrial glucose oxidation [22]. Overall, these findings are in accordance with the observations that UCP2 is commonly over-expressed in neoplastic tissues, as breast, ovarian, leukemia, bladder, esophagus, testicular, colorectal, kidney, pancreatic,

lung and prostate cancers [21] and that the glycolytic pathway is generally strongly enhanced in cancer cells [37].

Our recent studies demonstrated that mitochondrial uncoupling mediated by UCP2 inhibits autophagic cell death making pancreatic cancer cells particularly resistant to the anticancer drug gemcitabine [10, 15]. In a previous study, we have also functionally associated this phenomenon with the UCP2-mediated cytosolic stabilization of the glycolytic enzyme glyceraldehyde-3-phosphate dehydrogenase (GAPDH). Indeed, we revealed that ROS produced by inhibition of UCP2 are able to stimulate the oxidation of GAPDH glycolytic enzyme determining conformational changes, which favor its translocation into the nucleus where it can subsequently trigger the expression of cell death- and autophagy-related genes [15]. Therefore, UCP2 can prevent the activation of autophagic genes and concurrently stabilize the glycolytic enzyme GAPDH in the cytosol where glycolysis takes place making mitochondrial uncoupling a functional crossroad between Warburg effect, autophagy and ROS regulation. By proteomic profiling we here report in Table 1 that the expression of one form of nucleophosmin, a protein that regulates the nuclear translocation of the glycolytic enzyme glyceraldehyde 3-phosphate dehydrogenase (GAPDH) [38], decreased 2.56 fold after genipin treatment, supporting our previous data that stated the enhancement of GAPDH nuclear translocation in pancreas cancer cells after UCP2 inhibition [15], further proving novel insights in the stimulation of the Warburg effect by UCP2. In this context, we provide here further evidence and novel insights, schematically reported and summarized in **Figure 7**, concerning the crucial role of UCP2 on the metabolic shift from mtOXPHOS to glycolysis in pancreas cancer cells. By using a bidimensional proteomic approach and gene ontology classifications [39] we observed that the differentially expressed proteins after UCP2 inhibition are mainly related to metabolic processes. In particular, we revealed that UCP2 induces expression of hnRNPA2/B1 through its antioxidant function, suggesting its involvement in the up-regulation of both GLUT1 and pyruvate kinase isoform M2 (PKM2) resulting in enhanced lactate secretion. In addition to GLUT1 and PKM2 stimulation, we also reported in Table 1 that a form of LDH, a key

enzyme involved in L-lactic acid fermentation, emerged to be strongly downregulated (<20 fold) after UCP2 inhibition by genipin, thus supporting a role of UCP2 in the maintenance of the glycolytic phenotype of cancer cells [31, 32].

On the other side, the metabolic shift from mtOXPHOS to glycolysis, and the consequent enhanced sensitivity of cancer cells to the glycolysis inhibitor 2-DG, are further revealed by the UCP2-mediated repression of OXPHOS complexes expression/activity and oxygen consumption. Interestingly, mtDNA amount remains unchanged suggesting that OXPHOS inhibition by UCP2 is not due to mitochondria amount alteration. Finally, manganese superoxide dismutase (MnSOD) was found to be downregulated (-1.53 fold) after genipin treatment (Table 1), suggesting its involvement in the UCP2-mediated metabolic shift towards glycolysis in cancer cells. Indeed, it has been recently demonstrated that MnSOD upregulation in cancer cells established a steady flow of $H_2O_2$ originating from mitochondria that sustains AMP-activated kinase (AMPK) activation and the metabolic shift to glycolysis, indicating that the MnSOD/AMPK axis is critical to support the Warburg effect [40]. Furthermore, porin-1 (VDAC1), enhanced 1.4 fold after genipin treatment (Table 1), has been demonstrated to strongly modulate mitochondrial metabolism of cancer cells, beyond its role on mitochondrial autophagy [41].

Altogether our findings provide novel mechanistic insights into the metabolic regulation driven by UCP2 and unveil the inhibition of glycolysis pathway as a strategic therapeutic approach against UCP2-overexpressing human cancers.

**Acknowledgements**

This work was supported by Joint Projects program 2015 from University of Verona to M. Donadelli (n. B12I15002320003); by grant from Fondo de Investigaciones Sanitarias of Instituto de Salud Carlos III (PI12/01827 and PI14/01434) of the Spanish Government confinanced by FEDER-Unión Europea ("Una manera de hacer Europa"). I. Dando is a fellow of Fondazione Umberto Veronesi. E. Dalla Pozza is a fellow of AIRC 5 per mille (grant no. 12182). M. Torrens-Mas is a fellow of Ministerio de Educación, Cultura y Deporte of Spanish Government (FPU grant).

**Conflict of interest**

The authors declare that they have no conflicts of interest.

**Legends to Figures**

**Figure 1.** Effect of UCP2 inhibition on cell growth, reactive oxygen species production and mitochondrial membrane potential in PaCa44 cells. (**A**) Cell growth was measured by using Crystal Violet colorimetric assay. Cells were seeded in 96-well plates, incubated overnight, and treated with 150 μM genipin for 16 h and/or transfected with siUCP2. (**B**) PaCa44 cells were seeded in 96-well plates, incubated overnight, and treated with 150 μM genipin for 16 h. The fluorescence intensity of the MitoSox Red probe, corresponding to the level of mitochondrial superoxide production, was measured by using a multimode plate reader, as described in Material and Methods. (**C**) Mitochondrial membrane potential (ΔΨm) was measured fluorimetrically in PaCa44 cells treated with 150 μM genipin for 16 h or transfected with siUCP2 using TMRM, as described in Material and Methods. Values are the means ± SEM of three independent experiments each performed in triplicate. Statistical analysis: * $p<0.05$, ** $p< 0.01$, and *** $p<0.001$ genipin and/or siRNA UCP2 versus Ctrl, and genipin+siRNA UCP2 versus genipin.

**Figure 2.** UCP2 sensitizes PaCa44 cells to the treatment with the glycolytic inhibitor 2-deoxy-D-glucose (2-DG). Cells were seeded in 96-well plates and transfected for 48 h with siUCP2 or a nontargeting siRNA used as negative control (siCTRL) (**A**), or with the pCMV expression vector containing the human cDNA of UCP2 to overexpress UCP2 (o.e. UCP2) or with empty vector (mock) (**B**). For each experimental condition, cells were untreated or treated with 1, 2.5 or 5 μM 2-DG for 48 h. Cell growth was determined using the Crystal Violet colorimetric assay. The percentage of cell growth corresponds to the effect of 2-DG in each indicated transfection condition, as compared to its relative negative control. All values are expressed as means ± SEM of three independent experiments each performed in triplicate. Statistical analysis: * $p<0.05$ siUCP2 versus siCTRL; # o.e. UCP2 versus mock.

**Figure 3.** UCP2 induces Stathmin and hnRNPA2/B1 expression in PaCa44 cells. (**A**) PaCa44 cells were seeded in 60-mm diameter culture dishes and treated with 150 μM genipin for 16 h. 1D-WB analysis was performed with 50 μg of whole cell extracts, probed with the anti-stathmin antibody and PVDF membrane was stained with amido black for control loading. Whole cell extracts obtained as described above were used for 1D-WB (**B**) and 2D-WB (**C**) analyses of hnRNPA2/B1 isoforms. These analyses were representative of three biological replicates. For quantitative analysis, bands were scanned as digital peaks and the areas of the peaks were reported as fold change, as described in Material and Methods. (**D**) HnRNPA2/B1 mRNA expression analysis through qPCR in PaCa44 cells treated with 150 μM genipin for 16 h, or with siRNA UCP2 or the relative negative control (siCTRL), or with the pCMV expression vector containing the human cDNA of UCP2 to overexpress UCP2 (o.e. UCP2) or with empty vector (mock). All values are expressed as means ± SEM of three independent experiments each performed in triplicate. Statistical analysis: * $p<0.05$, ** $p<0.01$ and *** $p<0.001$ genipin versus Ctrl, or siRNA UCP2 versus siCTRL, or o.e. UCP2 versus mock.

**Figure 4.** UCP2 induces the expression of GLUT1 and PKM2 and the secretion of L-lactic acid in PaCa44 cells. (**A**) GLUT1 and PKM2 mRNA expression analysis through qPCR in PaCa44 cells treated with 150 μM genipin for 16 h, or with siRNA UCP2 or the relative negative control (siCTRL), or with the pCMV expression vector containing the human cDNA of UCP2 to overexpress UCP2 (o.e. UCP2) or with empty vector (mock). All values are expressed as means ± SEM of three independent experiments each performed in triplicate. (**B**) Cells were seeded in 60-mm diameter culture dishes and treated with 150 μM genipin for 16 h or (**C**) transfected with siRNA-UCP2 (siUCP2) or its non-targeting siRNA (siCTRL) as negative control. Western blotting was performed with 50 μg of proteins from whole cell extracts probed with the indicated antibodies.

This analysis was representative of three biological replicates. For quantitative analysis, bands were scanned as digital peaks and the areas of the peaks were reported as fold change, as described in Material and Methods. The value of GAPDH was used as a normalizing factor. Statistical analysis: * $p<0.05$ genipin versus CTRL; # $p<0.05$ siUCP2 versus siCTRL. (**D**) PaCa44 cells were set up and processed for IF analysis as detailed in the Material and Methods. GLUT1 protein was revealed by reaction with the specific primary antibody and the secondary antibody conjugated with Alexa Fluor 488. These images are representative of three separate experiments for PaCa44 cells untreated (control) or treated with 150 μM genipin for 16 h. 2D pictures were taken by means of a Leica TCS-SP5 LCM. Nuclei in blue (DAPI) and anti-GLUT1 in green. In the insert box the differential GLUT1 expression levels is highlighted. Scale bar, 20 μm. (**E**) PaCa44 cells were transfected with the plasmid over-expressing UCP2 for 48 h. L-lactic acid level in the culture medium has been analysed by measuring the absorbance at 340nm and the L-lactic acid concentration has been calculated, as detailed in Materials and Methods. Here we report the fold change of the L-lactic acid concentration secreted in the culture medium of cells overexpressing UCP2 versus cells transfected with a mock vector. Statistical analysis: * $p<0.05$ and ** $p<0.01$ genipin versus Ctrl, siUCP2 versus siCTRL, o.e. UCP2 versus mock.

**Figure 5.** UCP2 induces hnRNPA2/B1 and PKM2 through its antioxidant function. PaCa44 cells were seeded in 60-mm diameter culture dishes and treated with 150 μM genipin and/or 20 mM NAC for 16 h. Western blotting was performed with 50 μg of proteins from whole cell extracts probed with the indicated antibodies. This analysis was representative of three biological replicates. For quantitative analysis, bands were scanned as digital peaks and the areas of the peaks were reported as fold change, as described in Material and Methods. The value of amido black staining was used as a normalizing factor. A dashed line delineates cut parts from the same western blot membrane. Statistical analysis: * $p<0.05$, ** $p<0.01$ and *** $p<0.001$ genipin, or NAC or genipin+NAC versus CTRL; or genipin+NAC versus genipin.

**Figure 6.** UCP2 inhibits mitochondrial OXPHOS and oxygen consumption in Panc1 cells. (**A**) Cells were seeded in 6-well plates and transfected with siUCP2 for 4 h at 37 ºC and 5% CO2. Cells were further grown for 48 h and harvested for Western Blot analysis, which has been performed on V-ATP5A-54 kDa (Complex V, subunit alpha), III-UQCRC2-48 kDa (Complex III, subunit Core 2), II-SDHB-29 kDa (Complex II, subunit 30 kDa), IV-COX II-22 kDa (Complex IV, subunit II), and I-NDUFB8-18 kDa (Complex I, subunit NDUFB8). For quantitative analysis, bands were scanned as digital peaks and the areas of the peaks were reported as fold change, as described in Material and Methods. (**B**) COX activity (complex IV) and (C) ATPase activity (complex V) were measured by spectrophotometric methods. (**D**) DNA was extracted from Panc1 cells and a qPCR was performed for a nuclear gene (18S) and a mitochondrial gene (NADH dehydrogenase subunit 4). Values are expressed as the ratio mitochondrial/nuclear gene. (**E**) Basal respiration was measured for 7 min. Maximal respiration was calculated as the difference between the rate after FCCP (8 μM) addition and the rate after antimycin (1 μM) addition. ATP production was calculated as the difference between basal respiration rate and rate after oligomycin addition. Finally, difference between rate after oligomycin addition and rate after antimycin addition was attributed to proton leak. All values are expressed as means ± SEM of three independent experiments each performed in duplicate. Statistical analysis: * $p<0.05$ siUCP2 versus CTRL.

**Figure 7.** Schematic representation of the main metabolic mechanisms regulated by UCP2 identified in this study. Dashed line: multistep reaction. Full line: direct reaction. Italic: enzyme. Green arrow/box: activated pathway/enzyme by UCP2. Red arrow/box: inhibited pathway/enzyme by UCP2. (*): experimentally demonstrated in the present study. Acronyms: Glyceralehyde-3 phosphate: G3P; Glyceralehyde-3 phosphate dehydrogenase: GAPDH; 1,3-biphosphoglycerate: 1,3bisPG; phosphoenolpyruvate: PEP; pyruvate kinase isoform M2: PKM2; pyruvate: PYR; lactate

dehydrogenase: LDH; mtOXPHOS: mitochondrial oxidative phosphorylation; ROS: reactive oxygen species.

## Legends to Supplementary Figures

**Supplementary Figure 1.** UCP2 mRNA expression levels after UCP2 silencing or overexpression. PaCa44 cells were transfected with (**A**) siRNA UCP2 or the relative negative control (siCTRL), or (**B**) with the pCMV expression vector containing the human cDNA of UCP2 (o.e. UCP2) or with empty vector (mock). All values are expressed as means ± SEM of three independent experiments each performed in triplicate. Statistical analysis: * $p<0.05$ siUCP2 versus siCTRL, or o.e. UCP2 versus mock.

**Supplementary Figure 2.** Effect of 2-DG on PaCa44 cells presenting UCP2 overexpression or knock-down. Panc1 cells were seeded in 96-well plates and transfected for 48 h with pCMV expression vector containing the human cDNA of UCP2 (o.e.UCP2) or with siUCP2. Cell growth was determined by Crystal Violet colorimetric assay. The rate of cell growth inhibition corresponds to the effect of 2.5 mM 2-DG for 48 h as compared to untreated cells, in each indicated transfection condition. Three independent experiments each performed in triplicate were performed for each assay condition. Statistical analysis: * $p<0.05$ o.e.UCP2 or siRNA UCP2 versus Ctrl.

**Supplementary Figure 3.** Representative two-dimensional gel electrophoresis images of PaCa44 cells (**A**) untreated or (**B**) treated with 150 μM genipin for 16 h.

**Supplementary Figure 4.** PANTHER functional classification of the 19 differentially expressed proteins after treatment with the UCP2 inhibitor genipin in pancreas cancer PaCa44 cells. Pie charts show the classification according to (**A**) cellular component, (**B**) biological process and (**C**) molecular function.

**Supplementary Figure 5.** Oxygen consumption rate for control and siUCP2-transfected Panc1 cells. Basal rate was measured and then components modulating mitochondrial function were added sequentially: oligomycin 1 µM, FCCP 8 µM and antimycin 1 µM. Statistical analysis: * $p<0.05$ siUCP2 versus Ctrl.

## References


1 Mailloux, R. J. and Harper, M. E. (2012) Mitochondrial proticity and ROS signaling: lessons from the uncoupling proteins. Trends in endocrinology and metabolism: TEM. **23**, 451-458

2 Pazos, P., Lima, L., Tovar, S., Gonzalez-Touceda, D., Dieguez, C. and Garcia, M. C. (2015) Divergent responses to thermogenic stimuli in BAT and subcutaneous adipose tissue from interleukin 18 and interleukin 18 receptor 1-deficient mice. Scientific reports. **5**, 17977

3 Echtay, K. S. (2007) Mitochondrial uncoupling proteins--what is their physiological role? Free radical biology & medicine. **43**, 1351-1371

4 Toda, C. and Diano, S. (2014) Mitochondrial UCP2 in the central regulation of metabolism. Best practice & research. Clinical endocrinology & metabolism. **28**, 757-764

5 Donadelli, M., Dando, I., Fiorini, C. and Palmieri, M. (2014) UCP2, a mitochondrial protein regulated at multiple levels. Cellular and molecular life sciences : CMLS. **71**, 1171-1190

6 Donadelli, M., Dando, I., Dalla Pozza, E. and Palmieri, M. (2015) Mitochondrial uncoupling protein 2 and pancreatic cancer: a new potential target therapy. World journal of gastroenterology : WJG. **21**, 3232-3238

7 Lopez-Bernardo, E., Anedda, A., Sanchez-Perez, P., Acosta-Iborra, B. and Cadenas, S. (2015) 4-Hydroxynonenal induces Nrf2-mediated UCP3 upregulation in mouse cardiomyocytes. Free radical biology & medicine. **88**, 427-438

8 Ramsden, D. B., Ho, P. W., Ho, J. W., Liu, H. F., So, D. H., Tse, H. M., Chan, K. H. and Ho, S. L. (2012) Human neuronal uncoupling proteins 4 and 5 (UCP4 and UCP5): structural properties, regulation, and physiological role in protection against oxidative stress and mitochondrial dysfunction. Brain and behavior. **2**, 468-478

9 Derdak, Z., Fulop, P., Sabo, E., Tavares, R., Berthiaume, E. P., Resnick, M. B., Paragh, G., Wands, J. R. and Baffy, G. (2006) Enhanced colon tumor induction in uncoupling protein-2 deficient mice is associated with NF-kappaB activation and oxidative stress. Carcinogenesis. **27**, 956-961

10 Dalla Pozza, E., Fiorini, C., Dando, I., Menegazzi, M., Sgarbossa, A., Costanzo, C., Palmieri, M. and Donadelli, M. (2012) Role of mitochondrial uncoupling protein 2 in cancer cell resistance to gemcitabine. Biochimica et biophysica acta. **1823**, 1856-1863

11 Pons, D. G., Nadal-Serrano, M., Torrens-Mas, M., Valle, A., Oliver, J. and Roca, P. (2015) UCP2 inhibition sensitizes breast cancer cells to therapeutic agents by increasing oxidative stress. Free radical biology & medicine. **86**, 67-77

12 Pfefferle, A., Mailloux, R. J., Adjeitey, C. N. and Harper, M. E. (2013) Glutathionylation of UCP2 sensitizes drug resistant leukemia cells to chemotherapeutics. Biochimica et biophysica acta. **1833**, 80-89

13 Derdak, Z., Mark, N. M., Beldi, G., Robson, S. C., Wands, J. R. and Baffy, G. (2008) The mitochondrial uncoupling protein-2 promotes chemoresistance in cancer cells. Cancer research. **68**, 2813-2819

14 Brand, M. D. and Esteves, T. C. (2005) Physiological functions of the mitochondrial uncoupling proteins UCP2 and UCP3. Cell Metab. **2**, 85-93

15 Dando, I., Fiorini, C., Pozza, E. D., Padroni, C., Costanzo, C., Palmieri, M. and Donadelli, M. (2013) UCP2 inhibition triggers ROS-dependent nuclear translocation of GAPDH and autophagic cell death in pancreatic adenocarcinoma cells. Biochimica et biophysica acta. **1833**, 672-679

16 Vyas, S., Zaganjor, E. and Haigis, M. C. (2016) Mitochondria and Cancer. Cell. **166**, 555-566

17 Brandi, J., Dando, I., Palmieri, M., Donadelli, M. and Cecconi, D. (2013) Comparative proteomic and phosphoproteomic profiling of pancreatic adenocarcinoma cells treated with CB1 or CB2 agonists. Electrophoresis. **34**, 1359-1368

18 Dalla Pozza, E., Donadelli, M., Costanzo, C., Zaniboni, T., Dando, I., Franchini, M., Arpicco, S., Scarpa, A. and Palmieri, M. (2011) Gemcitabine response in pancreatic adenocarcinoma cells is synergistically enhanced by dithiocarbamate derivatives. Free radical biology & medicine. **50**, 926-933

19 Kalyanaraman, B., Darley-Usmar, V., Davies, K. J., Dennery, P. A., Forman, H. J., Grisham, M. B., Mann, G. E., Moore, K., Roberts, L. J., 2nd and Ischiropoulos, H. (2012) Measuring reactive oxygen and nitrogen species with fluorescent probes: challenges and limitations. Free radical biology & medicine. **52**, 1-6

20 Robinson, K. M., Janes, M. S. and Beckman, J. S. (2008) The selective detection of mitochondrial superoxide by live cell imaging. Nat Protoc. **3**, 941-947
21 Ayyasamy, V., Owens, K. M., Desouki, M. M., Liang, P., Bakin, A., Thangaraj, K., Buchsbaum, D. J., LoBuglio, A. F. and Singh, K. K. (2011) Cellular model of Warburg effect identifies tumor promoting function of UCP2 in breast cancer and its suppression by genipin. PLoS One. **6**, e24792
22 Zhang, J., Khvorostov, I., Hong, J. S., Oktay, Y., Vergnes, L., Nuebel, E., Wahjudi, P. N., Setoguchi, K., Wang, G., Do, A., Jung, H. J., McCaffery, J. M., Kurland, I. J., Reue, K., Lee, W. N., Koehler, C. M. and Teitell, M. A. (2011) UCP2 regulates energy metabolism and differentiation potential of human pluripotent stem cells. The EMBO journal. **30**, 4860-4873
23 Nie, W., Xu, M. D., Gan, L., Huang, H., Xiu, Q. and Li, B. (2015) Overexpression of stathmin 1 is a poor prognostic biomarker in non-small cell lung cancer. Laboratory investigation; a journal of technical methods and pathology. **95**, 56-64
24 Feng, W., Xiaoyan, X., Xuan, Y., Xiangke, L., Zichang, Y., Ran, Z., Liuxing, W. and Qingxia, F. (2015) Silencing stathmin-modulating efficiency of chemotherapy for esophageal squamous cell cancer with paclitaxel. Cancer gene therapy. **22**, 115-121
25 Jiang, L., Chen, Y., Chan, C. Y., Wang, X., Lin, L., He, M. L., Lin, M. C., Yew, D. T., Sung, J. J., Li, J. C. and Kung, H. F. (2009) Down-regulation of stathmin is required for TGF-beta inducible early gene 1 induced growth inhibition of pancreatic cancer cells. Cancer letters. **274**, 101-108
26 David, C. J., Chen, M., Assanah, M., Canoll, P. and Manley, J. L. (2010) HnRNP proteins controlled by c-Myc deregulate pyruvate kinase mRNA splicing in cancer. Nature. **463**, 364-368
27 Griffin, M. E., Hamilton, B. J., Roy, K. M., Du, M., Willson, A. M., Keenan, B. J., Wang, X. W. and Nichols, R. C. (2004) Post-transcriptional regulation of glucose transporter-1 by an AU-rich element in the 3'UTR and by hnRNP A2. Biochemical and biophysical research communications. **318**, 977-982
28 Li, Q., Liu, X., Yin, Y., Zheng, J. T., Jiang, C. F., Wang, J., Shen, H., Li, C. Y., Wang, M., Liu, L. Z. and Jiang, B. H. (2014) Insulin regulates glucose consumption and lactate production through reactive oxygen species and pyruvate kinase M2. Oxidative medicine and cellular longevity. **2014**, 504953
29 Zhu, J., Bi, Z., Yang, T., Wang, W., Li, Z., Huang, W., Wang, L., Zhang, S., Zhou, Y., Fan, N., Bai, Y., Song, W., Wang, C., Wang, H. and Bi, Y. (2014) Regulation of PKM2 and Nrf2-ARE pathway during benzoquinone induced oxidative stress in yolk sac hematopoietic stem cells. PLoS One. **9**, e113733
30 Dando, I., Dalla Pozza, E., Biondani, G., Cordani, M., Palmieri, M. and Donadelli, M. (2015) The metabolic landscape of cancer stem cells. IUBMB life. **67**, 687-693
31 Stine, Z. E., Walton, Z. E., Altman, B. J., Hsieh, A. L. and Dang, C. V. (2015) MYC, Metabolism, and Cancer. Cancer discovery. **5**, 1024-1039
32 Xu, Y., Miriyala, S., Fang, F., Bakthavatchalu, V., Noel, T., Schell, D. M., Wang, C., St Clair, W. H. and St Clair, D. K. (2015) Manganese superoxide dismutase deficiency triggers mitochondrial uncoupling and the Warburg effect. Oncogene. **34**, 4229-4237
33 Cho, Y. S., Lee, J. H., Jung, K. H., Park, J. W., Moon, S. H., Choe, Y. S. and Lee, K. H. (2016) Molecular mechanism of (18)F-FDG uptake reduction induced by genipin in T47D cancer cell and role of uncoupling protein-2 in cancer cell glucose metabolism. Nuclear medicine and biology. **43**, 587-592
34 Mailloux, R. J. and Harper, M. E. (2011) Uncoupling proteins and the control of mitochondrial reactive oxygen species production. Free radical biology & medicine. **51**, 1106-1115
35 Vozza, A., Parisi, G., De Leonardis, F., Lasorsa, F. M., Castegna, A., Amorese, D., Marmo, R., Calcagnile, V. M., Palmieri, L., Ricquier, D., Paradies, E., Scarcia, P., Palmieri, F., Bouillaud, F. and Fiermonte, G. (2014) UCP2 transports C4 metabolites out of mitochondria, regulating glucose and glutamine oxidation. Proc Natl Acad Sci U S A. **111**, 960-965
36 Samudio, I., Fiegl, M., McQueen, T., Clise-Dwyer, K. and Andreeff, M. (2008) The warburg effect in leukemia-stroma cocultures is mediated by mitochondrial uncoupling associated with uncoupling protein 2 activation. Cancer research. **68**, 5198-5205
37 Mikawa, T., ME, L. L., Takaori-Kondo, A., Inagaki, N., Yokode, M. and Kondoh, H. (2015) Dysregulated glycolysis as an oncogenic event. Cellular and molecular life sciences : CMLS. **72**, 1881-1892
38 Lee, S. B., Kim, C. K., Lee, K. H. and Ahn, J. Y. (2012) S-nitrosylation of B23/nucleophosmin by GAPDH protects cells from the SIAH1-GAPDH death cascade. The Journal of cell biology. **199**, 65-76

39 Cecconi, D. and Zamo, A. (2011) Proteomics of human cancer tissues and cells. Trac-Trend Anal Chem. **30**, 346-359

40 Hart, P. C., Mao, M., de Abreu, A. L., Ansenberger-Fricano, K., Ekoue, D. N., Ganini, D., Kajdacsy-Balla, A., Diamond, A. M., Minshall, R. D., Consolaro, M. E., Santos, J. H. and Bonini, M. G. (2015) MnSOD upregulation sustains the Warburg effect via mitochondrial ROS and AMPK-dependent signalling in cancer. Nature communications. **6**, 6053

41 Maldonado, E. N., Sheldon, K. L., DeHart, D. N., Patnaik, J., Manevich, Y., Townsend, D. M., Bezrukov, S. M., Rostovtseva, T. K. and Lemasters, J. J. (2013) Voltage-dependent anion channels modulate mitochondrial metabolism in cancer cells: regulation by free tubulin and erastin. J Biol Chem. **288**, 11920-11929

**Table 1**

**Table 1.** 2-DE gel identified proteins in PaCa44 cells by nano-HPLC-Chip ion trap MS/MS. [a)] Mascot score: the protein score obtained by the sum of the highest ions score for each distinct sequence; [b)] Amino acid sequence coverage for the identified protein; [c)] Fold change: the expression ratios between the means of spots value (% vol) at two samples resulting from digital image analysis. + Indicates increased protein intensity and – indicates decreased protein intensity; nd = not-detected (< 20 fold of variation).

| Protein name | Gene name | NCBI acc. # | No. of peptides identified | Mascot score [a)] | Mr. (Da) exp./theor. | pI exp./theor. | Sequence Coverage [b)] (%) | Cellular component GO term | Biological process GO term | Molecular function GO term | Genipin / control fold change [c)] | t test (p value) | p (corr) VIP>1.5 |
|---|---|---|---|---|---|---|---|---|---|---|---|---|---|
| alpha-enolase isoform 1 | ENO1 | gi\|4503571 | 15 | 490 | 50000 / 47139 | 8 / 7.01 | 37 | nucleus, cytosol | glucose metabolic process; regulation of transcription | transcription corepressor activity | + 1.35 | 0.015 | 0.748 |
| cytokeratin 8 | KRT8 | gi\|181573 | 6 | 223 | 60000 / 53529 | 7 / 5.52 | 12 | intermediate filament | cytoskeleton organization | protein binding | + 1.41 | 0.017 | 0.726 |
| F-actin-capping protein subunit beta isoform | CAPZB | gi\|4826659 | 3 | 53 | 27000 / 30609 | 5.5 / 5.69 | 8 | cytoskeleton | regulation of cell morphogenesis | protein binding | - 1.43 | 0.006 | - 0.800 |
| heterogeneous nuclear ribonucleoproteins A2/B1 | HNRNP A2B1 | gi\|4504447 | 5 | 170 | 31000 / 35984 | 9 / 8.67 | 13 | nucleus, cytosol | mRNA processing | nucleotide binding | n.d. | 0.026 | - 0.887 |
| L-lactate dehydrogenase A chain | LDHA | gi\|2600997 25 | 2 | 80 | 30000 / 30037 | 8.5 / 8.27 | 8 | cytosol, mitochondrion | glycolysis | oxidoreductase activity | n.d. | 0.004 | - 0.888 |
| manganese superoxide dismutase (MnSOD) | SOD2 | gi\|34709 | 2 | 51 | 25000 / 24720 | 8 / 8.35 | 6 | mitochondrion | response to reactive oxygen species | superoxide dismutase activity | - 1.53 | 0.005 | - 0.697 |
| nucleolar phosphoprotein B23 (nucleophosmin) | NPM1 | gi\|825671 | 7 | 139 | 30000 / 30919 | 4.5 / 4.71 | 12 | nucleus | DNA repair | nucleic acid binding | - 2.56 | 0.013 | / |
| nucleoside diphosphate kinase A (Nm23 protein) | NME1 | gi\|35068 | 3 | 122 | 20000 / 20398 | 6.5 / 7.07 | 22 | nucleus, mitochondrion | nucleoside diphosphate phosphorylation | nucleic acid binding | + 1.46 | 0.004 | 0.836 |
| porin 1 | VDAC1 | gi\|238427 | 3 | 51 | 30000 / 30623 | 9 / 8.63 | 7 | mitochondrion | apoptotic process | protein binding | + 1.4 | 0.012 | 0.692 |
| prostaglandin E synthase 3 | PTGES3 | gi\|2330857 9 | 3 | 147 | 25000 / 14861 | 4.5 / 5.09 | 24 | nucleus | signal transduction | telomerase activity | - 4.9 | 0.011 | - 0.693 |
| protein disulfide-isomerase | P4HB | gi\|2007012 5 | 3 | 185 | 60000 / 57081 | 4 / 4.76 | 7 | microsome, endoplasmic reticulum, Golgi | protein folding, metabolic process | oxidoreductase activity | n.d. | 0.001 | - 0.983 |
| protein disulfide-isomerase A3 | PDIA3 | gi\|860986 | 6 | 256 | 60000 / 56644 | 6 / 6.10 | 14 | phagocytic vesicle, endoplasmic reticulum | protein folding, metabolic process | oxidoreductase activity | - 1.66 | 0.007 | - 0.793 |
| stathmin 1 | STMN1 | gi\|5031851 | 2 | 61 | 18000 / 17292 | 6 / 5.76 | 13 | cytosol | signal transduction | signal transducer activity | - 1.37 | 0.003 | - 0.782 |
| tau-tubulin kinase | TTBK | gi\|2745160 2 | 1 | 69 | 30000 / 22329 | 6 / 4.80 | 5 | nucleus | signal transduction | protein kinase activity | + 2.03 | 0.004 | 0.851 |
| T-complex protein 1 | CCT2 | gi\|5453603 | 4 | 114 | 60000 / 57452 | 7 / 6.01 | 8 | nucleus, cytosol | cellular protein metabolic process | protein binding | + 1.41 | 0.017 | 0.726 |
| triosephosphate isomerase | TPI1 | gi\|136066 | 2 | 65 | 26000 / 26609 | 7 / 7.10 | 11 | nucleus, cytosol | glucose metabolic process | protein binding | + 1.72 | 0.001 | 0.829 |
| tropomyosin alpha-3 chain | TPM3 | gi\|1907264 9 | 1 | 48 | 29000 / 28792 | 4.7 / 4.72 | 4 | cytoskeleton | cellular component movement | actin binding | - 3.54 | 0.004 | / |
| Tu translation elongation factor, mitochondrial | TUFM | gi\|704416 | 2 | 60 | 50000 / 49509 | 8 / 7.7 | 5 | mitochondrion | translational elongation | elongation factor activity | + 1.88 | 0.011 | 0.816 |
| tyrosine--tRNA ligase, cytoplasmic | YARS | gi\|4507947 | 3 | 54 | 59106 / 60000 | 6.61 / 8 | 4 | nucleus, cytosol, extracellular space | apoptotic process, signal transduction | nucleic acid binding, signal transducer activity | + 3.49 | 0.001 | 0.867 |

**Figure 1**

Click here to download high resolution image

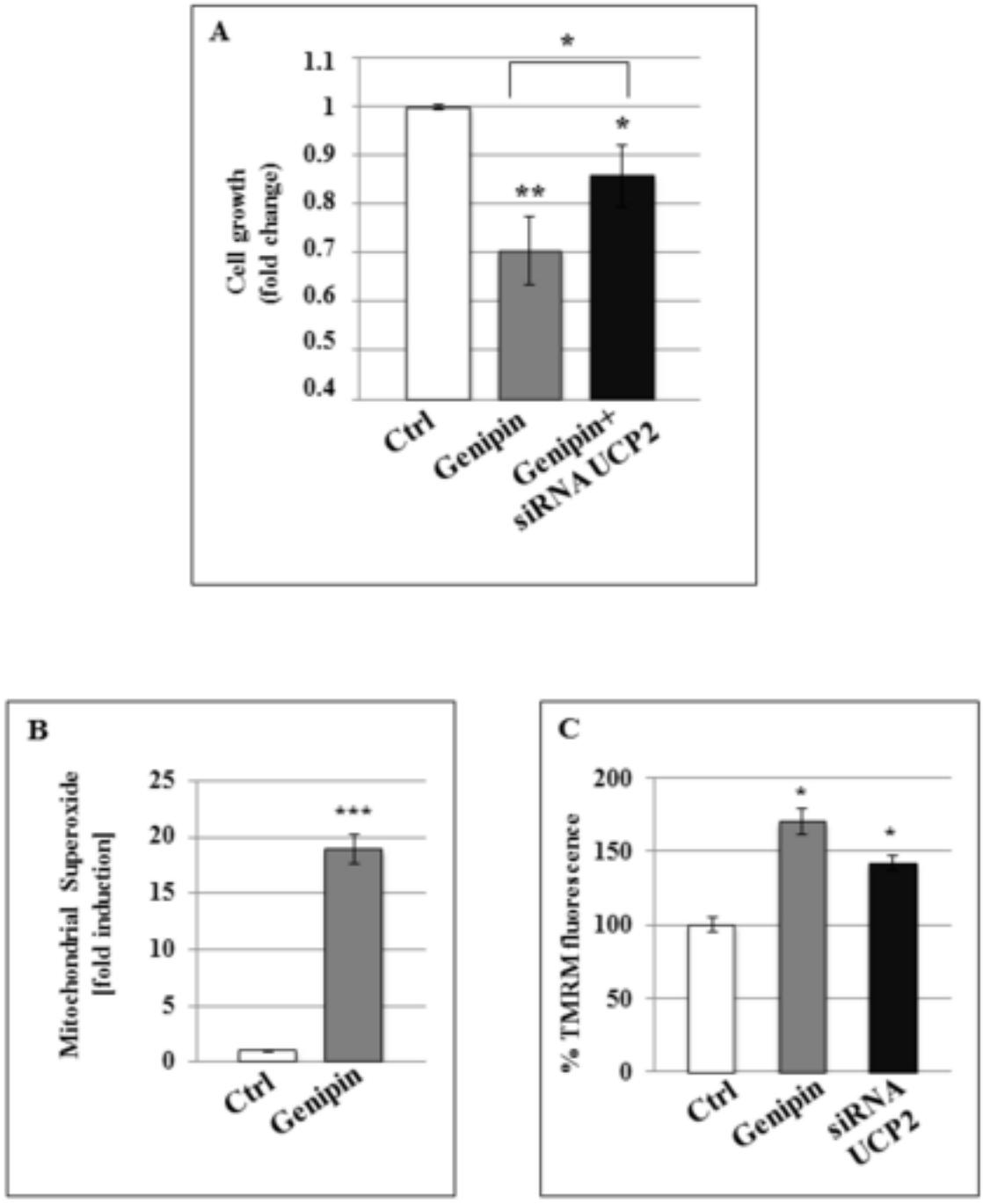


**Figure 1**

Figure 2
Click here to download high resolution image

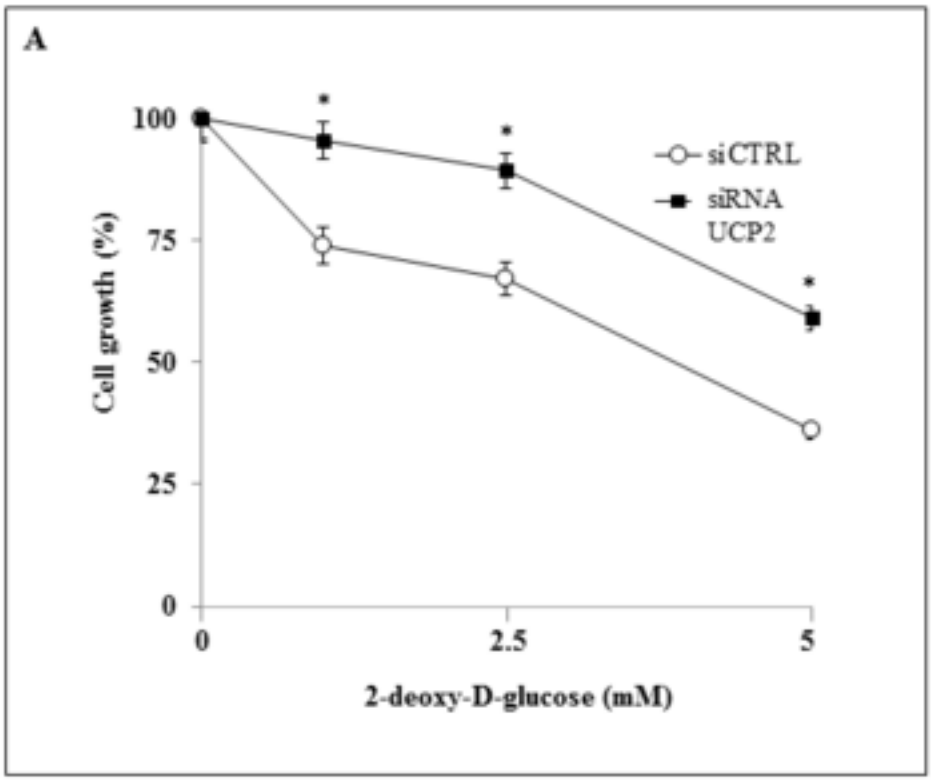


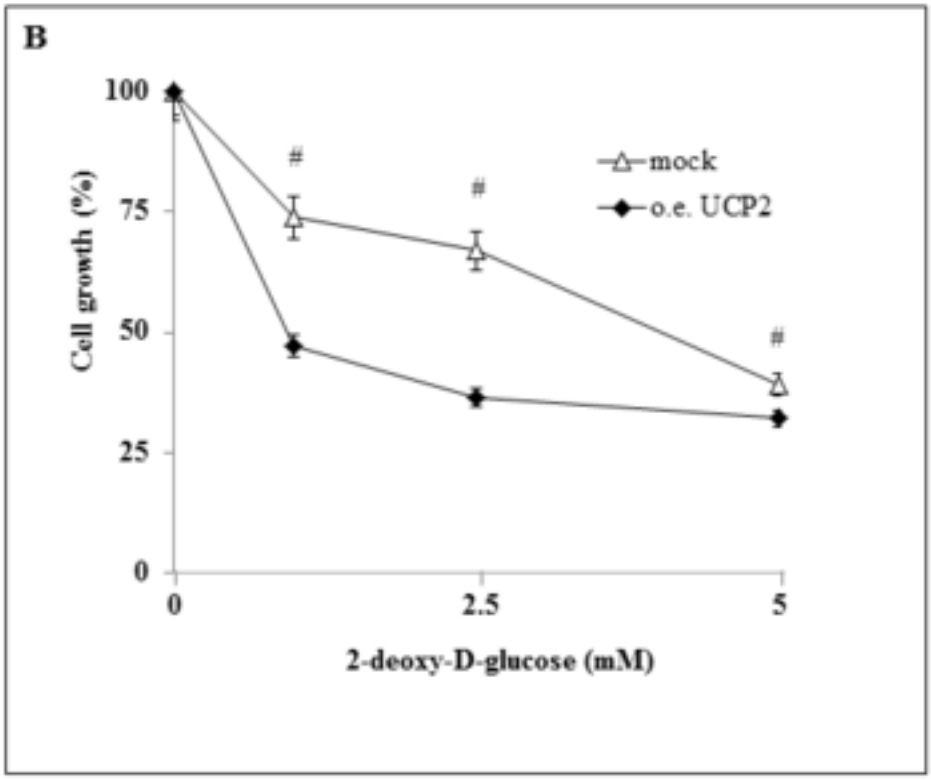


Figure 2

Figure 3

Click here to download high resolution image

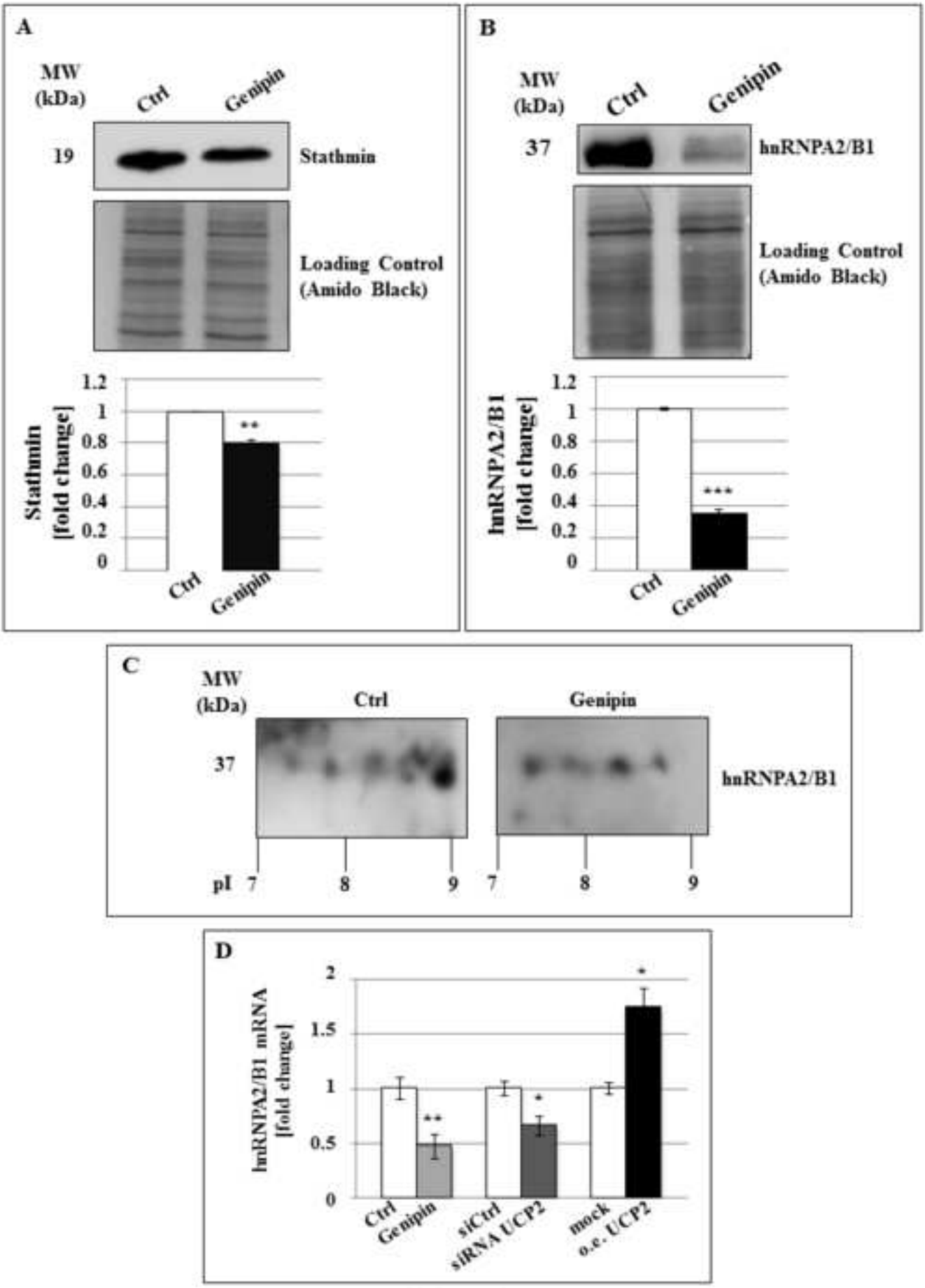


Figure 3

Figure 4

Click here to download high resolution image

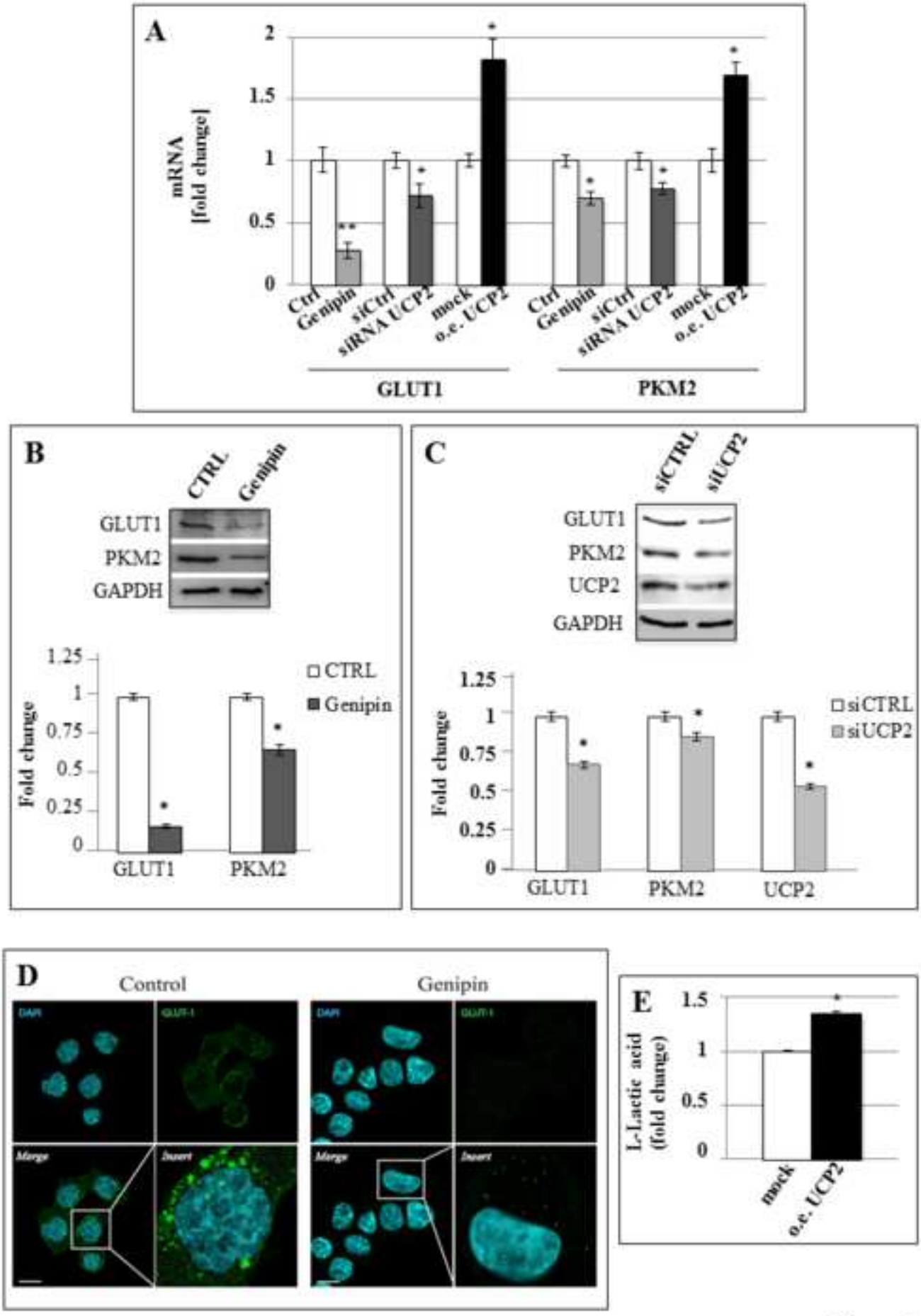


Figure 4

**Figure 5**

Click here to download high resolution image

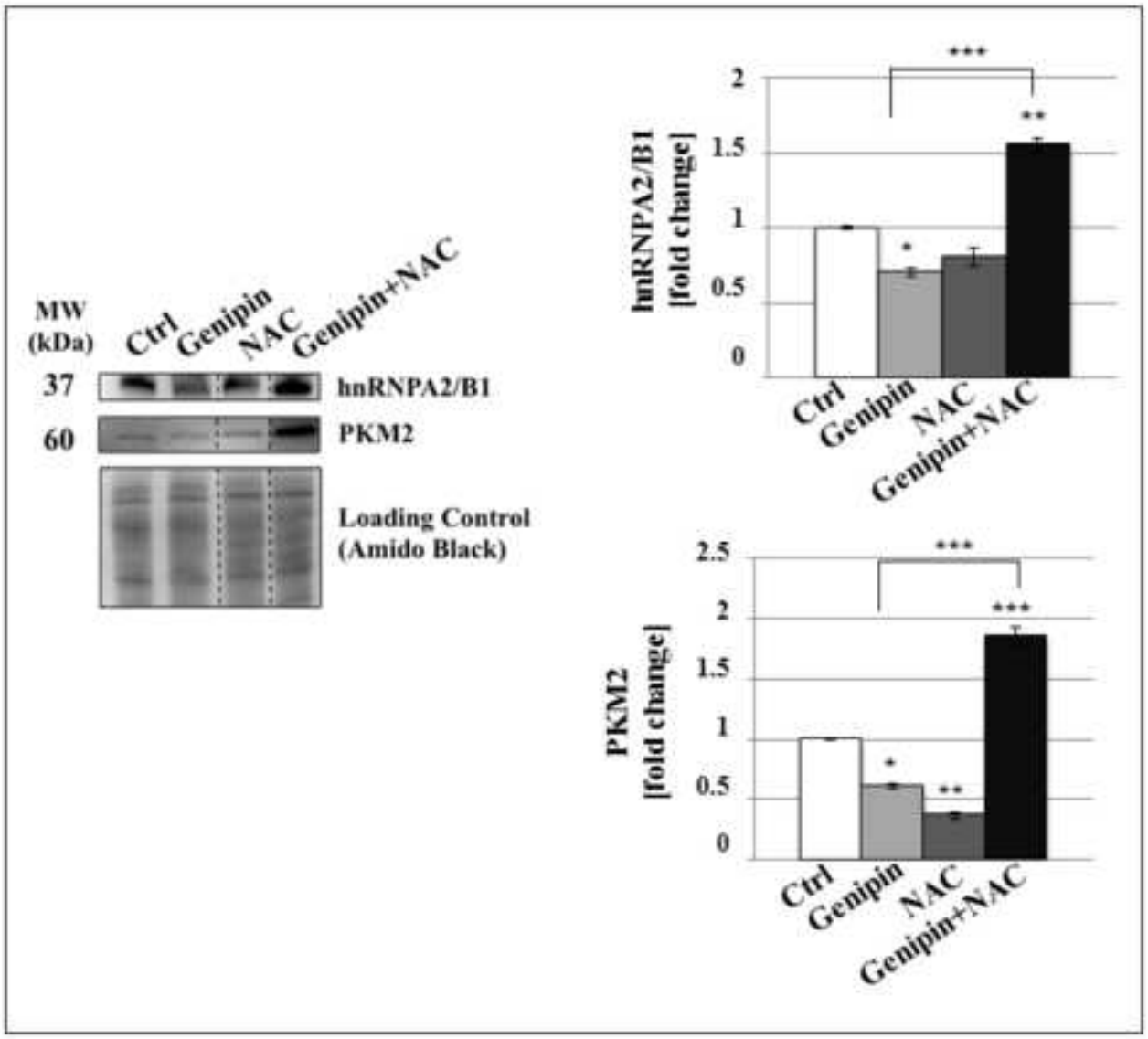


Figure 5

Figure 6

Click here to download high resolution image

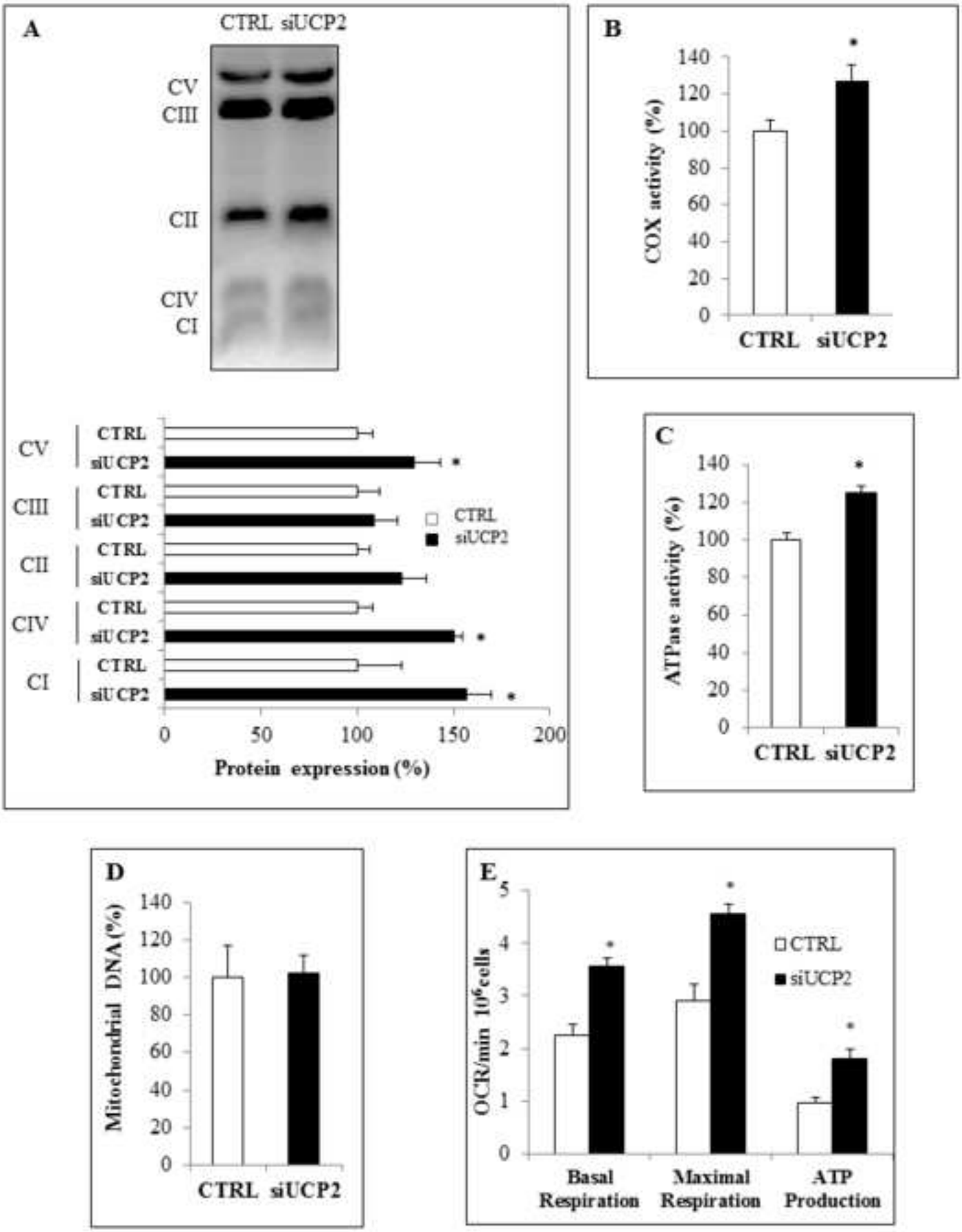


Figure 6

Figure 7
Click here to download high resolution image

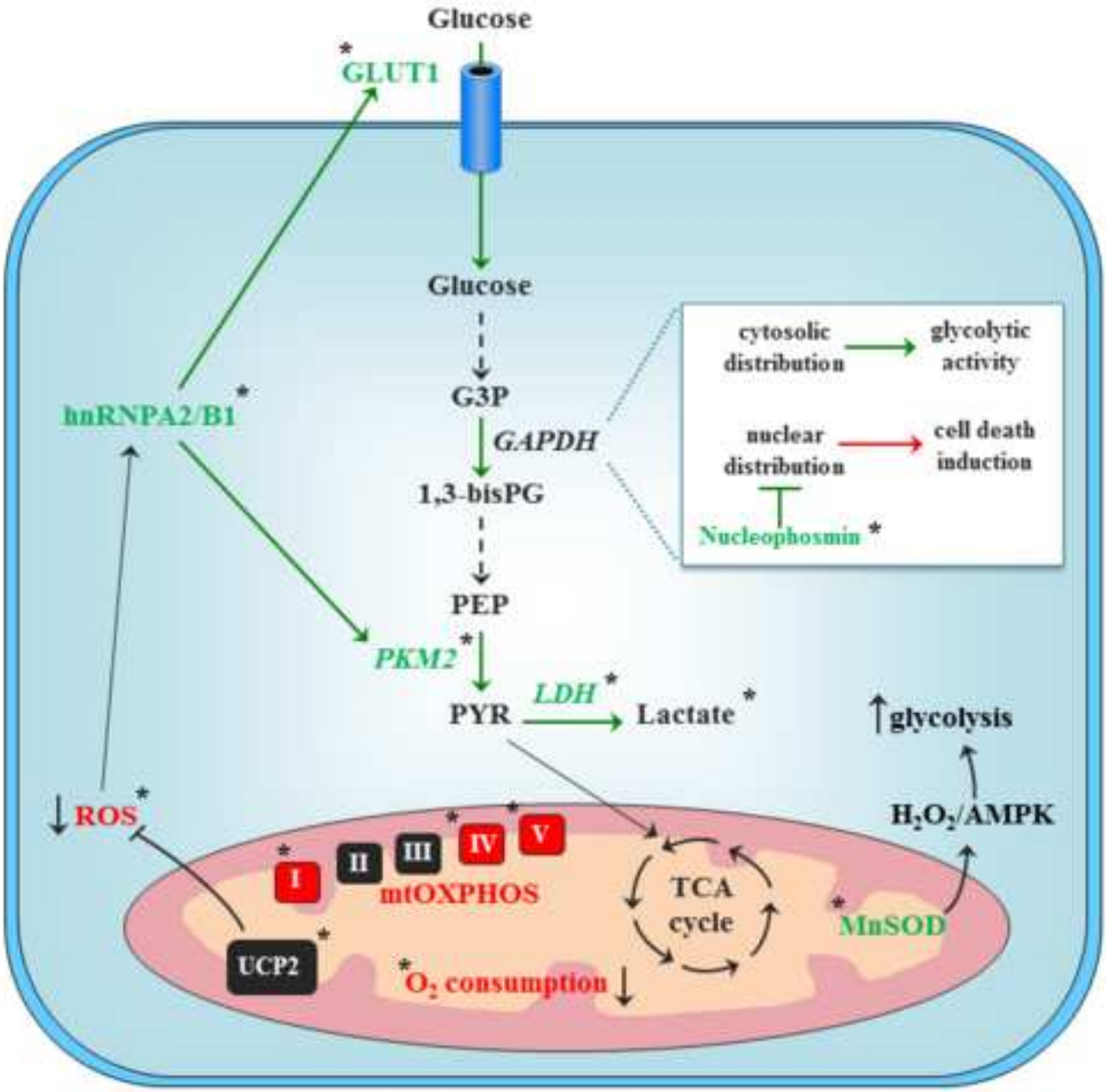


Figure 7

**Supplementary Figure 1**

**Click here to download Supplementary Material: Suppl. Fig. 1.tif**

**Supplementary Figure 2**

**Click here to download Supplementary Material: Suppl. Fig. 2.tif**

**Supplementary Figure 3**

Click here to download Supplementary Material: Suppl. Fig. 3.tif

**Supplementary Figure 4**

Click here to download Supplementary Material: Suppl. Fig. 4.tif

**Supplementary Figure 5**

Click here to download Supplementary Material: Suppl. Fig. 5.tif